# Development and Characterization of Vertically Aligned Metallized Carbon Fiber Composites

**Dilkaram Singh Ghuman**

**A Thesis**

**in**

**The Department**

**of**

**Mechanical, Industrial and Aerospace Engineering**

**Presented in Partial Fulfillment of the Requirements**

**for the Degree of**

**Master of Applied Science (Mechanical Engineering) at**

**Concordia University**

**Montréal, Québec, Canada**

**June 2025**

CONCORDIA UNIVERSITY

School of Graduate Studies

This is to certify that the thesis prepared

By: **Dilkaram Ghuman**
Entitled: **Development and Characterization of Vertically Aligned Metallized Carbon Fiber Composites**

and submitted in partial fulfillment of the requirements for the degree of

**Master of Applied Science (Mechanical Engineering)**

complies with the regulations of this University and meets the accepted standards with respect to originality and quality.

Signed by the Final Examining Committee:

_____ Chair
*Dr. Moussa Tembely*

_____ External Examiner
*Dr. Kelly Meek*

_____ Examiner
*Dr. Moussa Tembely*

_____ Supervisor
*Dr. Pantcho Stoyanov*

Approved by _____
Martin D. Pugh, Chair
Department of Mechanical, Industrial and Aerospace Engineering

June 18, 2025

_____
Mourad Debbabi, Dean
Faculty of Engineering and Computer Science

# Abstract


**Development and Characterization of Vertically Aligned Metallized Carbon Fiber Composites**

**Dilkaram Singh Ghuman**

The primary objective of this study was to conduct a comparative analysis of coatings produced using Atmospheric Plasma Spray (APS) and High Velocity Air Fuel (HVAF) processes, applied with Ti-6Al-4V and Sn powders. The coatings were deposited onto a single layer of low-melting polyaryletherketone (LMPAEK) reinforced with vertically aligned carbon fibers (ZRT film). Prior to the application of the spray coating, the samples underwent an electroless plating process with nickel, copper, or silver to serve as interlayers. A systematic comparison was conducted across various combinations of plating metals, thermal spray methods, and coating powders, including unplated baseline samples. The coated samples were characterized using scanning electron microscopy (SEM), confocal laser scanning microscopy (CLSM), and energy dispersive X-ray spectroscopy (EDS). Micro-CT scanning was employed to assess coating porosity. Thermal properties, including thermal conductivity, thermal resistance, and thermal diffusivity, were evaluated using a Thermal Interface Material Analyzer (TIMA). The study demonstrates that optimized thermally sprayed coatings can significantly improve the performance of composite materials, offering enhanced surface and mechanical properties suitable for scalable applications in high-performance, thermally sensitive industries.

# Acknowledgments

We want to thank Boston Materials for their great support and collaboration throughout this project. Your expertise and resources have been instrumental in helping us achieve our research goals.

We also acknowledge the generous support provided by Mitacs, whose funding has played a crucial role in facilitating this research endeavor. Their commitment to fostering innovation and academic-industry partnerships has been greatly appreciated.

Special thanks are due to Jim Barker from Artcraft Plating for his insightful contributions and technical guidance. Their capability to electroplate any material has enriched our research efforts and contributed significantly to the success of this project.

We are immensely grateful for the collaborative spirit and expertise brought by everyone involved, without them this project would not have been possible.

# Contents

# List of Figures

# List of Tables

# Organization of the Thesis

- Chapter 1 introduces the project by defining the thesis scope and purpose of the research.

- Chapter 2 provides a review of the current literature on metal matrix composites (MMCs) and carbon fiber-reinforced polymers (CFRPs), as well as techniques for metallizing carbon fiber composites. It also outlines methods for characterizing metalized samples.

- Chapter 3 presents the metallization of LMPAEK-reinforced carbon fiber composites aligned in the normal direction via electroless plating and thermal spraying. The study compares the roughness of the coatings and their tribological properties for Sn and Ti-6Al-4V (deposited with APS and HVAF), as well as for nickel, copper, and silver (electroless plated).

- Chapter 4 summarizes the research and suggests future studies on the use of normal-direction carbon fibers in metal and polymer matrix composites with metal coatings.

# Chapter
# 1. Introduction & Scope

*This chapter presents an introduction, as well as the overall scope and purpose of this thesis.*

# 1.1 Introduction

As the demand for higher processing power chips increases to enable faster computing for artificial intelligence (AI) and machine learning (ML), the heat released from transistors becomes a bottleneck for system performance. The energy dissipation from the high density of transistors limits the peak performance achievable with traditionally used materials. Selecting an efficient thermal interface material (TIM) therefore becomes crucial for cooling these microchips. The metallization of carbon fiber offers the potential to enhance both mechanical and thermal properties compared to conventional materials used in the industry.

Although composite materials show promise as alternatives, challenges persist regarding development costs, manufacturability, reliability, and performance outcomes. Many of these challenges are due to the novelty of these materials, which makes outcomes unknown. Balancing these factors while advancing the performance of metal matrix composites is a complex task. Due to manufacturing complexity, the development of normal-orientation composites remains a niche area, with limited knowledge available about different carbon fiber–reinforced metals and their properties. Much research has established a framework for understanding the evolution and mechanical properties of carbon fiber–reinforced polymers [1]. However, these studies have primarily focused on parallel and anti-parallel fiber orientations, whereas fibers oriented in the normal direction have been shown to offer superior mechanical performance [2].

This study aims to investigate a two-step metallization process that combines electroless plating and thermal spraying to deposit metallic coatings onto CFRP substrates with normal fiber orientation. The goal is to evaluate how different interlayer materials (Ni, Cu, Ag), coating powders (Sn, Ti-6Al-4V), and thermal spray methods (APS, HVAF) influence coating morphology, adhesion, and thermal performance. This work aims to address the current gap in literature regarding metallization of vertically aligned CFRP composites and proposes a scalable strategy for improving their functionality in high-performance, thermally sensitive applications.

# 1.2 Scope

The overall aim of this thesis is to develop and characterize vertically aligned metallized carbon fiber composites. Chapter 3 focuses on the metallization of a polymer matrix composite, achieved through electroless plating followed by thermal spraying. The scope of this chapter includes three key phases of the

project: development, characterization, and scale-up assessment.

## 1.3. Final remarks

Chapter 3 of this thesis has been published as an original research article titled *'Metallization of Carbon Fiber-Reinforced Polymers (CFRPs) Via a Two-Step Process of Electroless Plating and Thermal Spraying'* in the Journal of Thermal Spray Technology, published by Springer. The article is accessible online via DOI: 10.1007/s11666-025-01993-7.

# Chapter
# 2. Literature Review

*This chapter presents a literature review covering the fundamentals of tribology in soft metal coatings, alongside metal matrix composites and carbon fiber-reinforced polymers. It also investigates the current fiber coating techniques available in the market.*

# 2.1. Introduction of composite materials

## 2.1.1. Definition of composite materials

The term "composite material" is typically used to describe a substance that is composed of two or more distinct phases in contrast to monolithic materials which can be defined by their uniform and continuous microstructures [3], [4]. Metal alloys, ceramics and polymers can present limitations in terms of strength-to-weight ratio when employed in engineering design [4]. Whereas the composites optimize properties to create lighter yet tougher materials [5]. In its most fundamental configuration, the dispersed phase, such as stiff fibres, is embedded within a monolithic material, which is referred to as the matrix phase [3], [4]. Advances in technologies like additive manufacturing have driven the development of multiphase, man-made composite materials [4]. These materials are of topical interest in the field of engineering. As an example, in the aerospace industry, increasing interest to develop composite fan blades show they performs better than monolithic materials. However the earliest documented uses of these materials date back to the 16th century BCE where masons mixed straw and mud to create building blocks [6]. In the present era, composite materials are crafted with the objective of enhancing the combinations of mechanical characteristics, including stiffness, resilience, and strength in both ambient and high-temperature environments [4].

The composite material configurations can be classified into four principal categories: particle-reinforced, fibre-reinforced, structural, and nanocomposites [4]. Subsequently, each category is divided two geometrical classes. These terms describe different types of composite materials based on their properties, components, and uses. Additionally, the properties of composites can be influenced by the characteristics of particles in the dispersed phase including concentration, size, shape, distribution, and orientation [4]. The classifications are compiled and shown in Figure 1. The present study is primarily concerned with the fibre-reinforced composites that have been aligned and discontinuous, as indicated by the blue highlighting in the accompanying schematic. The fibre reinforcement is provided by the short carbon fibres that are aligned in the normal direction. The research proceeded with an investigation of both carbon-fibre reinforced polymers (CFRPs) and metal matrix composites (MMCs).

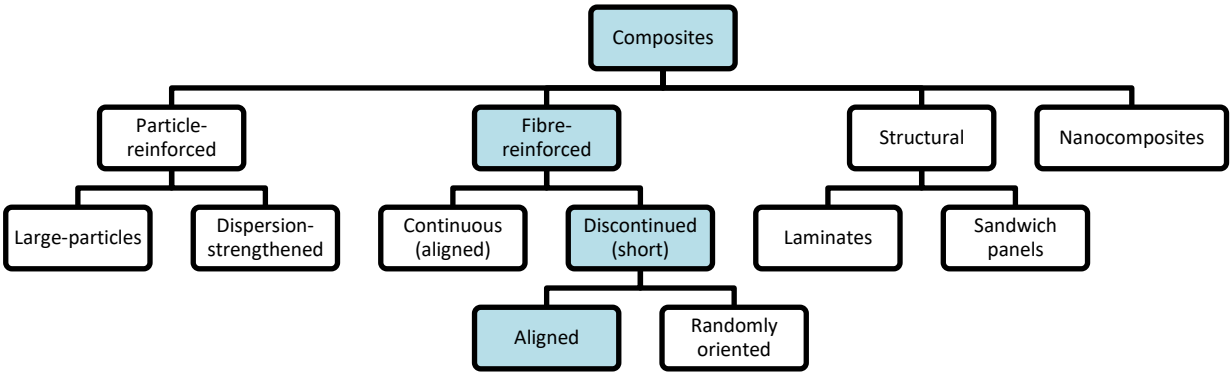


*Figure 1: Various classification scheme of composites [4]*

## 2.1.2. Reinforcement Types

As previously noted, the type of reinforcement is not solely contingent on the material in question, but is also subject to the influence of the geometric configuration of the dispersed phase [7]. The term "fibers" is used to describe a singular strand that exhibits a high length-to-diameter ratio, typically greater than 100 [8]. The agglomeration of fibres bundled as a group is referred to as a fibre tow or in short, a tow [9]. The increased surface area of the combined fibers allows the tensile force to be distributed along the fibers acting as the primary load-bearing component in composite materials [10].

The three most utilized categories of fibres are glass, carbon fibre and Kevlar. The glass fibre category encompasses classes with various chemical composition which modifies the physical properties of material. The E-glass class is distinguished by a relatively high silica content and a high aluminum oxide weight percentage, which contributes to its strength and excellent electrical insulating properties. Low elastic modulus carbon fibre (LM-CF) are characterized by their extremely high strength to weight ratio and stiffness to weight ratio as a result of the micro graphite crystal structure of the carbon fibers [11]. Kevlar fibers are part of aramid fibers where the fibers in question are composed of a long-chain synthetic polyamide, wherein a minimum of 85% of the amide linkages are attached directly to two aromatic rings [12]. The principal advantages of Kevlar fibres are their suitability for high-performance composite applications, where they offer the benefits of light weight, high strength and stiffness, damage resistance, and resistance to fatigue [13]. The commercially important fibres alongside their properties are presented in Table 1.

*Table 1: Mechanical properties of commercially important fibres [13]*

| Fibre Type | Fibre category | Density (g/cm$^3$) | Tensile strength (GPa) | Tensile modulus (GPa) |
|---|---|---|---|---|
| E-glass | Glass | 2.58 | 3.445 | 72.3 |
| LM-CF | Carbon | 1.45 | 3.5 | 200 |
| Kevlar 149 | Kevlar | 1.47 | 3.4 | 186 |

### 2.1.3. Matrix Materials

The matrix is the material that embeds the dispersed phase and plays several crucial roles in the functionality of composite materials. It serves to bind the fibers, thereby maintaining their position and ensuring the composite's structural integrity while protecting the fibers from the surrounding environment [4], [10]. The matrix provides an additional benefit in the form of load transfer and pressure distribution, which serve to relieve the force exerted on the fibers and provide thermal and electrical insulation [9]. This section aims to provide an overview of the three main categories of matrix material, namely polymers, metals, and ceramics [10]. The selection of the material for the matrix is based on the desired performance in the specific application environment and depends on factors such as mechanical, electrical, or thermal properties [7], [14].

An important factor influencing metallization is the orientation of the fibers. While the most commonly used fiber configurations are in the parallel directions to the plane of the substrate due to manufacturing convenience, the impact of fiber alignment in the normal direction on the metallization process has been investigated by Liberati et al., highlighting its significance in optimizing material performance [2].

### 2.1.4. Overview of Polymer, Metal and Ceramic Matrix Materials

Polymer matrices are organic materials that offer a relatively low cost compared to other materials, which makes them a popular choice for composites [10]. Thermoset and thermoplastic polymers are among the most commonly utilized materials for polymer matrix composites, primarily due to their straightforward manufacturing processes [15]. Thermosetting resins are a popular choice in the automotive industry due to their excellent mechanical properties and resistance to high temperatures and moisture [9]. Thermoplastic resins have the potential for future utilization in the aerospace industry for their insulating properties, with their tensile strength being a secondary consideration [5]. Examples of such materials include polyether

ether ketone (PEEK), low-melt polyaryletherketone (LMPAEK), polyphenylene sulfide (PPS), and polyetherimide (PEI) [4]. While there is no explicit standard regarding the matrix ratio of fiber quantity, sources such as Hyer indicate that the matrix resin typically constitutes 30 to 40% of the composite material [9].

The advancement of metal matrix composites (MMCs) was driven by the necessity for materials that could be utilized in military applications [16]. The combination of a nonmetallic material in a ductile metal matrix has gained traction in the recent years due to manufacturing advancement [17]. MMCs offer a number of advantages, including enhanced strength and stiffness, improved resistance to creep and fatigue, and elevated hardness, wear, and abrasion resistance. Furthermore, they can withstand higher operating temperatures [5].

The strength of ceramic matrices is maintained even at elevated temperatures, although this quality is accompanied by a weak toughness inherent to ceramic properties. To compensate for the weakness in brittleness, the addition of fibers is required in ceramic matrix composites (CMCs) [5]. The phenomenon of microcracking is more prevalent in CMC than in MMC or PMC, due to the considerably higher matrix failure strain compared to that observed in ceramics [18]. The adoption of CMCs in the aerospace industry is driven by the materials-related advantages they offer. These include high specific stiffness and strength, which reduce weight and fuel consumption, as well as lower fabrication and maintenance costs. Moreover, their capacity to function at elevated temperatures enhances thermal efficiency, while their durability prolongs the service life. Furthermore, their capacity for signature reduction enhances stealth technology by decreasing the detection range [18].

## 2.2. Metallization Processes for Composite Materials

This section examines the various metallization processes utilized in the fabrication of metal matrix composite materials or metallization of polymer matrix composites. The methods of metallization on carbon fibers (CFs) can be classified into two main categories: physical and chemical. The physical methods include sputtering, iron plating, and metal powder spraying, whereas the chemical methods encompass chemical plating and electroplating [19]. This research delves into the fundamental principles of electroless plating, thermal spray coating, and the prevalent metals employed for coating, elucidating their distinctive properties.

### 2.2.1. Electroless plating process overview

The electroplating of carbon fibers is a well-established process that has been the subject of extensive research, as evidenced by the work of Hua et al. [19] The fibers are immersed in a bath containing an electric current, which is conducted through an anode and results in the deposition of a metallic coating on the fibers [19]. While the electroplating process offers advantages such as accelerated deposition rates, cost-effectiveness, and suitability for conductive substrates, it is constrained by limitations including non-uniform coating on complex geometries and the inability to coat non-conductive surfaces without prior treatment such as the LMPAEK PMCs used in this study [19]. In contrast, the electroless plating process differs in that it enables uniform coating regardless of surface geometry and can deposit metals on non-conductive substrates through an autocatalytic chemical reaction without requiring an external power source [20]. Nevertheless, the electroless plating process has not been sufficiently developed or optimized for coating the Z-axis carbon fibers utilized in this study, which presents a challenge for its application in this context. Electroless plating is a well-established technique for coating non-conductive materials and intricate geometries. However, its application on Z-axis carbon fibers represents a relatively novel or specialized area of research.

### 2.2.2. Thermal Spray Process Overview

The field of thermal spray technologies for coatings has recently attracted a growing interest from researchers. Thermal spray technologies represent a diverse class of processes used to deposit coatings on substrates to improve their mechanical, thermal and functional properties. These processes are particularly important for composite materials, where surface treatments are critical for improving adhesion, thermal conductivity and wear resistance. Despite still representing an emerging field in composites science, thermal spray processes have shown immense potential and have attracted the interest of researchers seeking advanced metallization solutions.

#### 2.2.2.1. Types of Thermal Spray Processes

Thermal spray techniques can be broadly categorized into several distinct methods, including flame spraying, plasma spraying, arc spraying, cold spraying, and high-velocity air fuel (HVAF) spraying [21]. Each method is characterized by the specific energy source utilized to heat the coating material, along with the velocity at which the particles are propelled onto the substrate. The simplified classification for the

types of thermal spray processes in terms of temperature and velocity is depicted in Figure 2 [22].

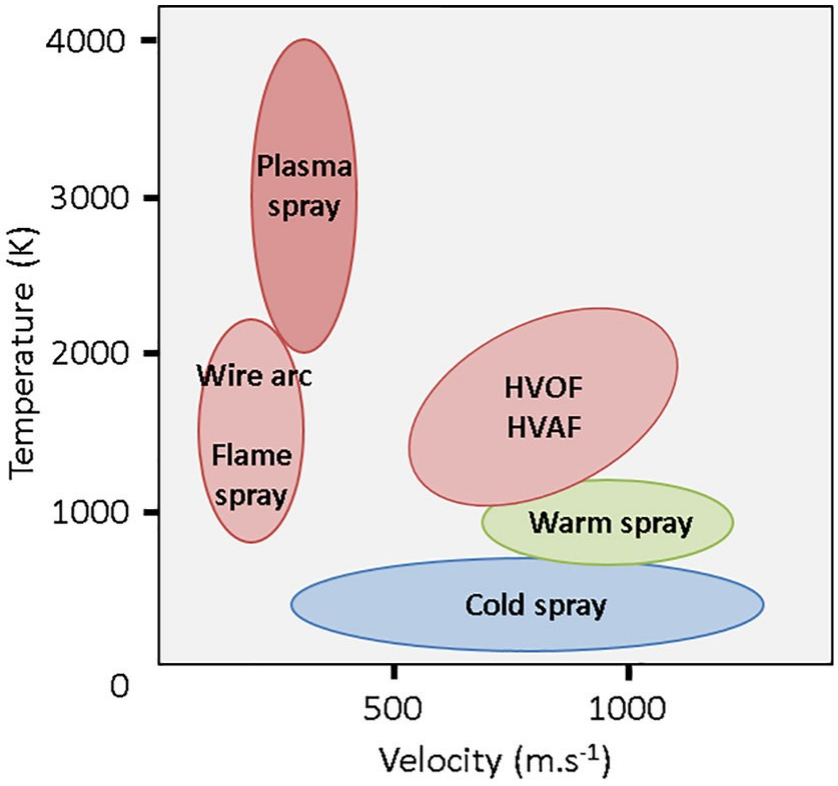


*Figure 2: Thermal Spray Categories [22]*

**Cold Spray**

Cold spray technique uses high-velocity gas jets to accelerate metallic powders toward the substrate at relatively low temperatures, preventing the thermal degradation of heat-sensitive materials [21]. Cold spray has become particularly relevant for polymer-based composites, where traditional high-temperature techniques may compromise structural integrity as demonstrated by Liberati et al. [2].

**HVAF Spraying**

The process of high-velocity air fuel spraying employs a high-temperature combustion procedure to propel particles to velocities exceeding the speed of sound. This method ensures the optimal adhesion and density of coatings while minimizing oxidation. The financial appeal of this process is clear, especially since air naturally contains approximately 21 vol.% oxygen, which can react with the fuel gas. The remaining portion

of the air then acts to cool the flame [21].

**Plasma Spraying**

Plasma spraying represents a coating technology that is notable for its versatility, allowing for the application of a wide range of materials, including refractory materials such as ceramics. Furthermore, it displays a high deposition rate, reaching up to several kilograms per hour, and is relatively straightforward to operate [23]. Plasma spraying involves the generation of a high-energy plasma jet, which melts and propels coating materials onto the substrate. Although this process is effective for the production of dense coatings, its high-temperature nature may restrict the range of applications for temperature-sensitive composite materials [21].

#### 2.2.2.2. Research Literature

Liberati et al. investigated the potential of utilizing the cold spray technique to deposit pure Sn coatings onto CFRPs, with a particular focus on composites with fibers oriented in the normal direction. The study demonstrated that the alignment of fibers facilitates deeper penetration of particles into the substrate, which in turn enhances coating adhesion and improves the overall performance of the composite material [2]. As Parmer et al. demonstrated, the incorporation of an interlayer through electroplating significantly enhances the adhesion between the metallic coating and the polymer substrate. The interlayer serves as a buffer, accommodating discrepancies in thermal expansion and enhancing mechanical bonding. Furthermore, it can serve as a foundation for enhanced compatibility with the metal layer, thereby increasing the durability and performance of the final coating. This approach is especially effective in cold spray applications, ensuring robust coating adhesion while minimizing damage to the polymer surface [24]. The application of HVAF (High-Velocity Air Fuel) spraying on electroless plated low-melting-point polyaryletherketone (LMPAEK) represents a novel approach, as yet untested. This innovative combination enhances adhesion and functionality, thereby paving the way for the development of advanced metallization techniques on thermoplastic polymer composites.

Despite the promising results, several challenges remain in the thermal spray metallization of composites. One primary issue is the mismatch in thermal expansion coefficients between the metallic coating and the polymer or carbon fiber substrate, which can lead to delamination under thermal cycling. Addressing this requires further optimization of interlayers and coating processes. Additionally, the microstructural integrity of the coating-substrate interface is crucial for ensuring long-term performance. Techniques such

as HVAF spraying, which minimize oxidation and thermal damage, are under active investigation to address these concerns.

### 2.2.3. Common Metals Used for Coatings and Their Properties

Current literature favors nickel deposition for electroless plating due to its ease of plating and well-established process [25]. Additionally, electroless nickel coatings offer excellent properties, such as corrosion resistance, wear resistance, and hardness, making them highly desirable for a wide range of applications. These factors contribute to the widespread use of nickel in electroless plating, particularly in industries like electronics, automotive, and aerospace [26]. This highlights the necessity for further research and development in the application of copper and silver coatings on carbon fiber.

Metals such as nickel, copper, silver and Sn and alloys such as Ti-6Al-4V are studied in this paper. Their relevant properties are shown in Table 2 alongside carbon fiber properties.

*Table 2: Properties of Materials Used in This Study.*

| | **Carbon Fiber** | **Nickel** | **Copper** | **Silver** | **Tin** | **Ti-6Al-4V** |
|---|---|---|---|---|---|---|
| Process Technique | Substrate (PMC or ZRT) | Electroless Plating | Electroless Plating | Electroless Plating | Thermal Spray | Thermal Spray |
| Thermal conductivity (W/m·K) | 10-233 [27] | 91 [28] | 391 [29] | 429 [29] | 66 [29] | 6.7 [30] |
| Thermal Expansion Coefficient ($10^{-6}$ m/m°C) | 1.2 [31] | 8.5 [29] | 17.6 [29] | 19.8 [29] | 23 [29] | 8.6 [30] |
| Surface Energy ($J/m^2$) | 0.08 [32] | 2.34 [33] | 1.37 [34] | 1.14 [35] | - | - |
| Melting Point (°C) | 3652 – 3697 [36] | 1455 [37] | 1085 [37] | 962 [37] | 232 [36] | 1604 – 1660 [30] |
| Viscosity at melting point (mPa·s) | - | 4.5 [38] | 4.4 [38] | 4.2 [38] | - | - |

## 2.3. Characterization Methods

The characterization techniques employed in this study were selected with the objective of providing a

comprehensive evaluation of the performance of composite materials. The key methodologies employed included scanning electron microscopy (SEM) and energy-dispersive spectroscopy (EDS), which were utilized to analyze fiber coatings and microstructural features. Micro-computed tomography (micro-CT) was employed to identify and quantify porosity, while confocal microscopy was used to assess surface roughness and detect cracks. Thermal conductivity was determined through laser flash analysis. These methods were grouped together to assess solderability, and thermal and mechanical thereby providing a comprehensive understanding of material performance.

## 2.5. Conclusion

The literature reviewed highlights the fundamental principles and recent advances in the field of composite materials, with a particular focus on fibre reinforced composites and their metallization processes. Composite materials have found applications in aerospace, automotive and other high-performance industries due to their customizable properties. The review categorizes composites based on their reinforcement type, matrix material and unique configurations, emphasizing the importance of fibre orientation in optimizing mechanical and thermal properties.

Metallization techniques, including electroless plating and thermal spraying, are critical to enhancing the functionality of composite materials, particularly for applications requiring improved thermal and electrical conductivity. While electroless plating is widely used for uniform coatings on non-conductive substrates, newer methods such as HVAF thermal spraying show promise for advanced applications, especially when combined with novel materials such as normal direction carbon fibres.

Despite these advancements, challenges remain, including optimizing adhesion in coatings, achieving uniform metallization on complex geometries, and understanding the interplay between process parameters and material performance. This study aims to address these gaps by exploring innovative metallization techniques and characterizing their impact on the structural and functional properties of polymer-reinforced composites and metal matrix composites.

The findings from this research have the potential to contribute to the development of high-performance composites with improved durability, efficiency and versatility of application, paving the way for future advances in materials science and engineering

# Chapter 3. Metallization of Carbon Fiber Reinforced Polymers (CFRPs) via a Two-Step Process of Electroless Plating and Thermal Spraying

*This study discusses metallization techniques for LMPAEK-reinforced carbon fiber composites aligned normally, using electroless plating and thermal spray. The chapter compares mechanical and thermal properties of Sn and Ti-6Al-4V (applied via APS and HVAF methods), and Ni, Cu, and Ag (electroless plated).*

## 3.1. Abstract

Carbon fiber-reinforced polymers (CFRPs) are commonly used materials within the aerospace industry due to their low density and favorable mechanical properties. Nevertheless, while CFRPs are optimal for applications requiring low weight and high strength, applying thermal spray coatings to these composites presents significant challenges, including distortion, oxidation, and poor coating adhesion. This study presents a new technique that combines electroless plating processes and thermal spray for depositing metals onto polymer-reinforced composites. The process addresses both the technical hurdles of bonding dissimilar materials and the need for lightweight, durable composites in aerospace manufacturing with low cost of production and high scalability. Samples of low-melt polyaryletherletone (LMPAEK) thermoplastic polymer reinforced with carbon fibers aligned in the normal direction (ZRT film) are plated with Ni, Cu, or Ag to provide an adhesion layer for the thermal spray processes. Subsequently, pure Sn and Ti-6Al-4V was deposited on the samples using High Velocity Air-Fuel (HVAF) and atmospheric plasma spray (APS) processes. Characterization of the samples was conducted to demonstrate the cracking in the Ti-6Al-4V coating on the Ni plating, which was attributed to the interlayers' thermal properties. Additionally, the variation in the coating thickness according to the interlayer, the thermal resistance of the resulting samples, and the splat morphology of the Sn and Ti-6Al-4V coatings were evaluated. Overall, the Sn coating applied via APS on the nickel plating exhibited the optimal performance in terms of the evaluated parameters in this study.

## 3.2. Introduction

Metallization of polymer matrix composites (PMCs) has gained significant interest within the past few decades due to its ability to enhance electrical and thermal conductivities, and provide electromagnetic interference shielding, erosion resistance, or radiation protection compared to uncoated PMCs [39] [40]. Previous research has established the foundation for depositing metal onto polymer matrix composites using various techniques such as vacuum depositions, electroplating or thermal spray [2], [41]. The use of metallic coatings can therefore improve the physical and thermal properties of carbon fiber reinforced polymers (CFRPs) while maintaining their mechanical properties. This makes them a desirable and cost-effective option for the aerospace industry's composite needs.

Thin film deposition techniques such as physical vapor deposition (PVD) and chemical vapor deposition (CVD) have limitations due to their high cost, maximum deposited material thickness (i.e. a few micrometers), and scalability challenges to larger components [2], [42]. Due to these limitations, a two-stage coating process was proposed by Parmar *et al.* [39] for the development of a metal coating for a polymer matrix composite. More specifically, throughout the first stage, a thin coating was formed to minimize the polymer deformation due to the impact of the particles followed by the coating build-up in the second stage [39]. Their extensive review article primarily focuses on the deposition process utilizing cold spray technology on composites of polyether ether ketone (PEEK) reinforced by carbon fiber. In addition, Audoit *et al.* [43] conducted a comprehensive test of the thermal, mechanical, and dielectric properties of low-melt polyaryletherletone (LMPAEK), which concluded that LMPAEK can maintain equivalent performance parameters to PEEK while requiring less energy to process at a lower temperature [43]. Similarly, Liberati *et al.* have shown the possibility of developing a pure Sn coating for CFRPs with fibers oriented in the normal direction using cold spray [2].

Previous studies established a foundation for metallic interlayers such as metallic meshing [44], [45] or electroplating/electroless plating of CFRPs [44]. However, little attention has been given to the possibility of using electroless plating combined with thermal spray techniques, such as Air Plasma Spray (APS) or High-Velocity Air Fuel (HVAF). These thermal spray processes present advantages in terms of improving the composites properties, extending the materials lifespan with a streamlined process and reducing manufacturing cost [46]. Additionally, the orientation of fibers in the normal direction in PMCs has also been shown to influence coating behavior in other deposition methods, such as cold-spray deposition [2]. Specifically, in the study of Liberati *et al.* [2], the deeper penetration of Sn into the substrate in cold spray has been linked to improved adhesion strength. These findings emphasize the broader influence of fiber

orientation on deposition techniques, providing a comparative context for evaluating APS and HVAF.

Thermal spraying is a versatile technique for applying coatings, offering advantages over traditional methods by enabling thicker coatings and reducing the need for solvents. Certain thermal spray processes, such as flame spraying and cold spray, can address processing limitations associated with other polymer coating techniques while minimizing environmental impact [47]. APS, with its high particle temperature, allows for precise control over particle melting, making it ideal for creating dense and uniform coatings [48]. HVAF, on the other hand, operates at lower particle temperatures but achieves higher particle velocities, reducing the risk of thermal degradation while maintaining high coating quality [49], [50]. These characteristics make APS and HVAF particularly effective for the deposition of metallic coatings onto polymer composites, where thermal sensitivity and coating adhesion are critical. Other processes, such as HVOF or cold spray with Ti-6Al-4V, pose challenges due to the material's limited plastic deformation, which can affect deposition efficiency and adhesion. Additionally, HVOF's higher process temperatures may require special modifications to prevent thermal damage to polymer composites [49], [51]. Although wire arc spraying operates at relatively lower temperatures than APS or HVOF, it was excluded due to challenges in achieving strong adhesion to the substrate. This is primarily due to the process's inherently lower bond strength, which results from higher porosity, larger particle sizes, and increased oxide content [52]. By focusing on APS and HVAF, this study aims to balance the competing demands of thermal management, coating adhesion, and deposition efficiency in metallizing polymer-reinforced composites.

While the benefits of APS and HVAF processes are well-established, the impact of combining electroless plating of a metal interlayer with these processes on low-melting polymer-reinforced carbon fiber composites has not been thoroughly investigated. Thus, the main purpose of this study is to investigate and identify optimal deposition processes for applying metallic coatings (i.e. Ti-6Al-4V and Sn) onto PMCs with fibers oriented in the normal direction as illustrated in Figure 3. In particular, the emphasis of this study is placed on comparing the APS and the HVAF processes. Ti-6Al-4V is widely used in the aerospace industry for engine part coatings [53], whereas Sn is a relatively cheap and readily available material that has successfully been sprayed onto CFRP and can serve as a point of comparison [53], [54], [55]. Each sample is plated via an electroless process with different metals (Ni, Cu, and Ag). The plating step is included to provide an interlayer between the substrate and the top coating, as explored by Fallah *et al.* [44]. The cross sections of the samples were imaged using FESEM to characterize the coating thickness. The pores were identified through micro-CT scanning. The surface roughness and presence of cracks were characterized using confocal microscopy. Finally, the thermal properties were also determined for the coated samples.

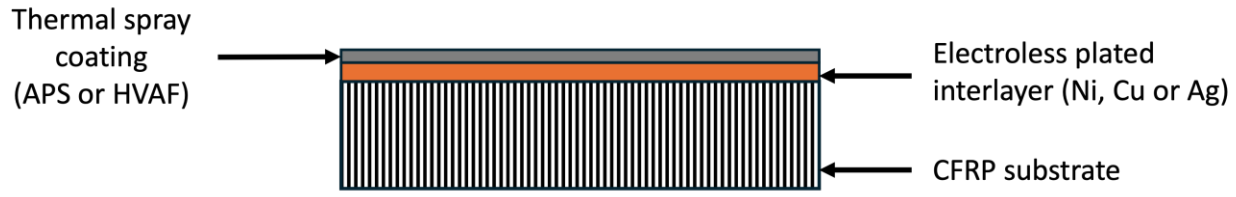


*Figure 3: Schematic of the produced sample cross-section*

## 3.3. Material and Methods

### 3.3.1. Substrate Material

The chosen substrate in this study was a CFRP material composed of normally oriented milled carbon fibers in an LMPAEK matrix provided by Boston Materials (Billerica, MA, USA). The samples used are a single layer of carbon fiber-low melting polyaryletherletone (CF-LMPAEK) (melting point of 303°C [56]) with a thickness of 200 μm and approximate dimensions of 2.54 cm by 2.54 cm.

### 3.3.2. Metallic Interlayer and Electroless Plating Process

Electroless plating is the process of depositing a continuous layer onto a catalytic surface through the interaction of a complex compound and a chemical reducing agent [57]. This process is characterized by its controlled autocatalytic nature. The resulting deposition allows for thin coating with a simple setup [57]. The electroless plating of the samples was carried out by Artcraft Plating (Burbank, CA, USA) to deposit Ni, Cu or Ag on CFRP. In order to plate using the electroless process, the surface is required to have a high electrochemical potential with an aqueous solution [58]. This process is inherently unstable and hinges on factors such as the substrate material, the pre-treatment process, the solution type, and the pH and temperature conditions to be stable during the plating process [59]. In this study, the metallic interlayer on the CF-LMPAEK composite is created by first preconditioning its surface with a neutralizing solution and then treating it with palladium chloride and stannous chloride, acting as reducing agents for palladium. The final step before plating involves removing the tin deposited with the stannous chloride to ensure better adhesion of the metals to the PMC. The sheets were flattened and affixed to a glass surface with tape and submerged into an aqueous solution for the deposition to occur. The initial steps were the same for all three metals that underwent electroless plating: Ni, Cu and Ag. The difference was in the plating solution used, which was specific to each metal. The samples were mounted on an aluminum sample holder using heat resistant tape, as shown in Figure 4, which displays the electroplated samples prior to the APS and HVAF processes.

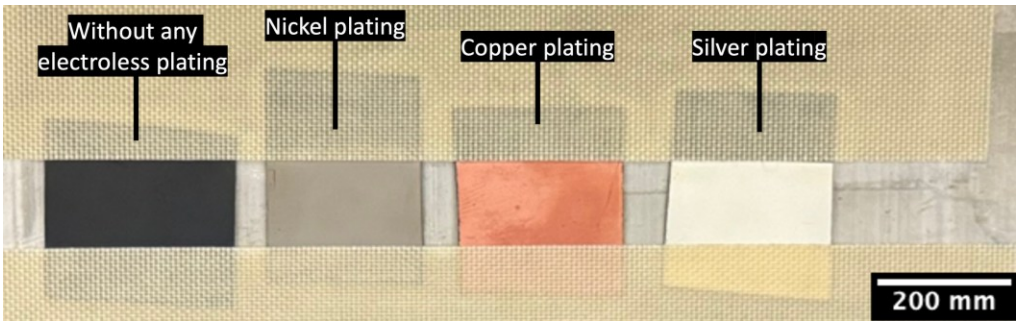


*Figure 4: Electroless plated samples before thermal spraying*

### 3.3.3. Feedstock Material and Spraying Conditions

For this study, the HVAF and APS processes were employed to deposit Sn and Ti-6Al-4V coatings onto CF-LMPEAK. The i7™ internal diameter HVAF spray gun (Uniquecoat Technologies LLC, Oilville, VA, USA), which operates on propylene, was used for the HVAF process. The internal-diameter HVAF system was selected because its design results in a lower thermal power output compared to standard outer-diameter systems [60]. This lower thermal power generated by the torch minimizes the heat transferred to the substrate, thereby reducing the risk of thermal degradation of the low-melting polymer composite while still maintaining sufficient particle velocity for effective coating deposition. The APS process utilized the 3MB plasma spray gun (Oerlikon, Switzerland). The detailed process parameters for both APS and HVAF are listed in Table 3 and Table 4, respectively. The parameters were maintained constant throughout the experimental process to minimize variability between the samples. However, the number of passes differed for the coating materials: one pass for Ti-6Al-4V and two passes for Sn.

*Table 3: APS process parameters*

| APS Parameters | |
|---|---|
| Primary plasma gas | 100% Ar |
| Argon flow rate | 60 L/min |
| Current | 400 A |
| Voltage | 34 V |
| Carrier gas | Ar (10 L/min) |
| Powder feed rate | 15 g/min |
| Spray distance | 80 mm |
| Gun traverse speed | 1 m/s |
| Overlap | 3 mm |

*Table 4: HVAF process parameters*

| HVAF Parameters | |
|---|---|
| Air pressure | 7.75 bar |
| Air flow rate | 2935 L/min |
| Propylene pressure | 6.5 bar |

| | |
|---|---|
| Propylene flow rate | 64 g/min |
| Carrier gas | Nitrogen (25 L/min) |
| Powder feed rate | 7 g/min |
| Spray distance | 80 mm |
| Gun traverse speed | 1 m/s |
| Overlap | 3 mm |

This experiment utilizes two distinct feedstock materials, namely Ti-6Al-4V (grade 5 titanium) and pure Sn, for both the APS and HVAF processes. The Ti-6Al-4V powder is obtained from AP&C (Boisbriand, QC, Canada), with a particle size ranging from 5 to 20 μm [11]. The Sn powder is sourced from CenterLine SST (Windsor, ON, Canada), and consists of spherical particles ranging from 5 to 45 μm in size [62]. The choice of pure tin powder has two advantages: first, it is soft metal that has been well-documented in literature and provides confirmed sprayability as opposed to most other materials [2], [54], [55]; second, it serves as a baseline for comparison with the selected titanium alloy. Ti-6Al-4V is composed of 90% titanium, 6% aluminium, and 4% vanadium [30]. The target spray area measures approximately 2.54 cm x 8.64 cm. Samples are secured on a 6.35 mm thick aluminium plate using heat-resistant tape. Finally, the plume characteristics, including the maximum particle velocity and particle temperature, were also measured during the HVAF spraying process (Accuraspray, Tecnar, Canada).

### 3.3.4. Sample Characterization

The observation and characterization of the samples can be performed from 4 perspectives: structural, surface, thermal and visual analysis. The structural analysis determines the presence of pores in the coating by micro-CT analysis using the Skyscan1172 instrument (MA, USA) and surface images using Scanning Electron Microscope (SEM) (Hitachi High Technologies America, Inc., USA). The analysis of the surface includes determining the surface roughness (arithmetical mean height, Sa) and analyzing the presence of cracks using the LEXT OLS4100 laser scanning confocal microscope (Olympus, Tokyo, Japan). For the surface roughness, multiple surface areas across the samples were sampled to account for surface variability. To improve data quality, waviness filters and noise reduction techniques were applied with the Lext software, ensuring accurate representation of the surface topography. The microscope is capable of measuring surface features at sub-micron levels, with a lateral resolution of 0.12 μm and a vertical resolution of 10 nm. In addition, cross-sectional imaging and elemental mapping were performed using FESEM (Hitachi High Technologies America, Inc., USA), which has the capability of performing Energy-Dispersive x-ray Spectroscopy (EDS) on the samples that were cold mounted in epoxy and polished. Furthermore, the micro-CT analysis was performed on a volume of approximately 2 mm x 6 mm for each sample, with the thickness varying depending on the specific sample. The technique used provided a resolution of 1 μm, which allowed for detailed visualization of internal features and porosity. The samples

were prepared by meticulously arranging them on a holder to ensure optimal alignment and to mitigate artifacts during the scanning process. Finally, the thermal resistances of the material were measured using the Thermal Interface Material Analyzer Model 5 (TIMA5) by Nanotest (Berlin, Germany). Thermal resistance measurements were conducted utilizing a sample size of 10 mm x 10 mm. The configuration consisted of copper thermocouples with individual samples positioned between them. The thermocouple applied a pressure of 60 psi, and the temperature was held at 85°C. To ensure consistency and accuracy, the measurement was repeated on three times.

## 3.4. Results

### 3.4.1. APS Sprayed CF-LMPAEK samples

#### 3.4.1.1. Surface Characterization

The surfaces of the coatings were examined by scanning electron microscopy (SEM) and the results are summarized in Figure 5. The images show the top surface of the samples, illustrating the covered area, surface morphology, and deposited particles. The Sn coatings predominantly exhibit flattened, disk-like splats, indicative of melting and spreading upon impact. This morphology results in a more uniform coating for all plated interlayers in this study. The lower porosity observed in Sn coatings, compared to Ti-6Al-4V coatings, suggests better cohesion and coverage, particularly on Ni-plated samples. In contrast, small clusters of Ti-6Al-4V particles on all respective sprayed samples are clumped together. The Ti-6Al-4V coatings show a mixture of spherical particles and irregular splats. These features suggest partial melting or insufficient spreading during deposition, which contributes to the clustering and agglomeration of particles observed across all samples. This behavior is more pronounced in coatings deposited without interlayers or on Cu- and Ag-plated substrates, where regions of exposed CFRP are evident. The coatings applied to the Ni interlayer exhibits improved deposition, as evidenced by the uniformity observed in both the Sn and Ti-6Al-4V samples. The Ni interlayer appears to enhance particle deposition by promoting better adhesion and splat formation, resulting in improved coating quality.

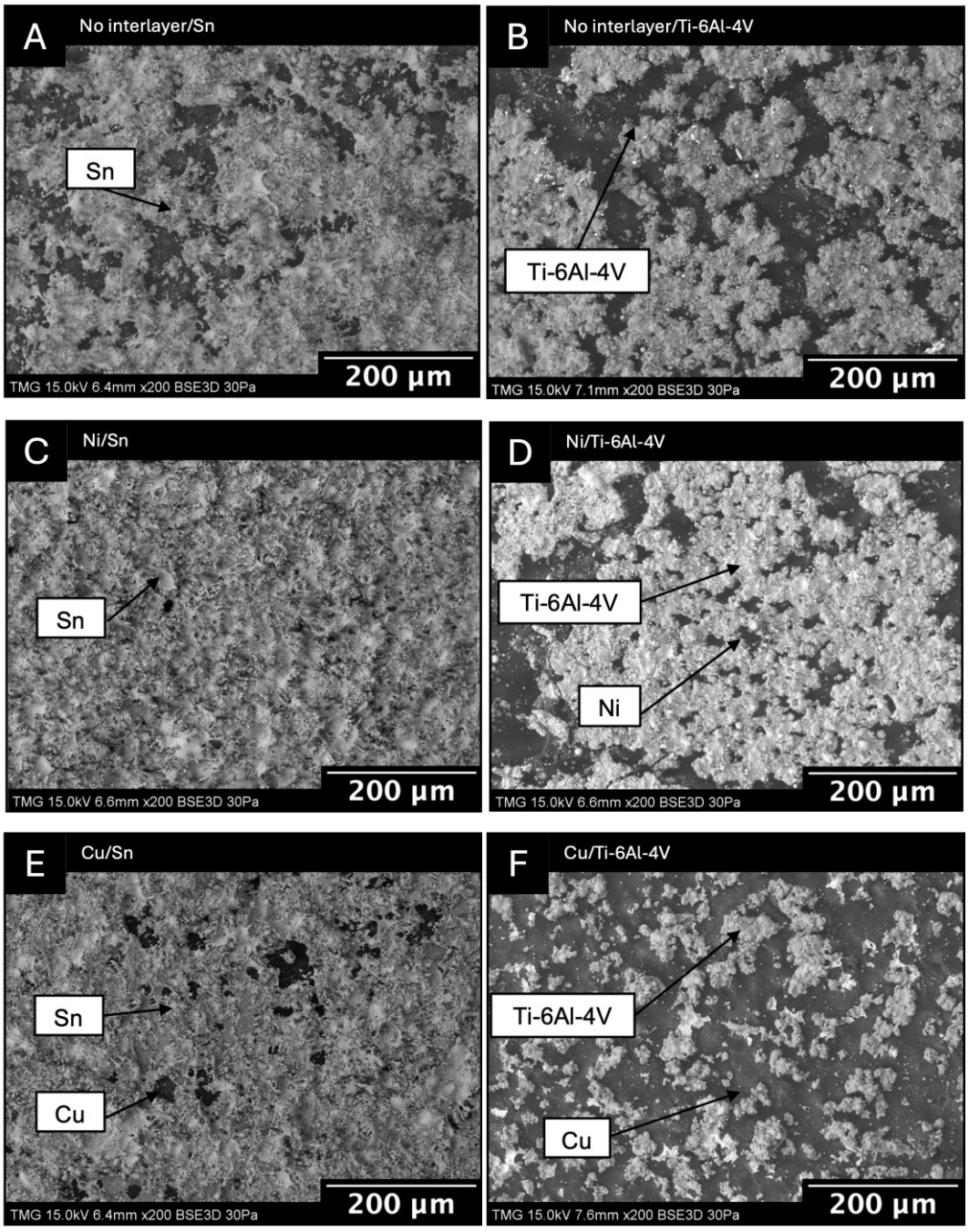
A
No interlayer/Sn
Sn
TMG 15.0kV 6.4mm x200 BSE3D 30Pa
200 µm
B
No interlayer/Ti-6Al-4V
Ti-6Al-4V
TMG 15.0kV 7.1mm x200 BSE3D 30Pa
200 µm
C
Ni/Sn
Sn
TMG 15.0kV 6.6mm x200 BSE3D 30Pa
200 µm
D
Ni/Ti-6Al-4V
Ti-6Al-4V
Ni
TMG 15.0kV 6.6mm x200 BSE3D 30Pa
200 µm
E
Cu/Sn
Sn
Cu
TMG 15.0kV 6.4mm x200 BSE3D 30Pa
200 µm
F
Cu/Ti-6Al-4V
Ti-6Al-4V
Cu
TMG 15.0kV 7.6mm x200 BSE3D 30Pa
200 µm

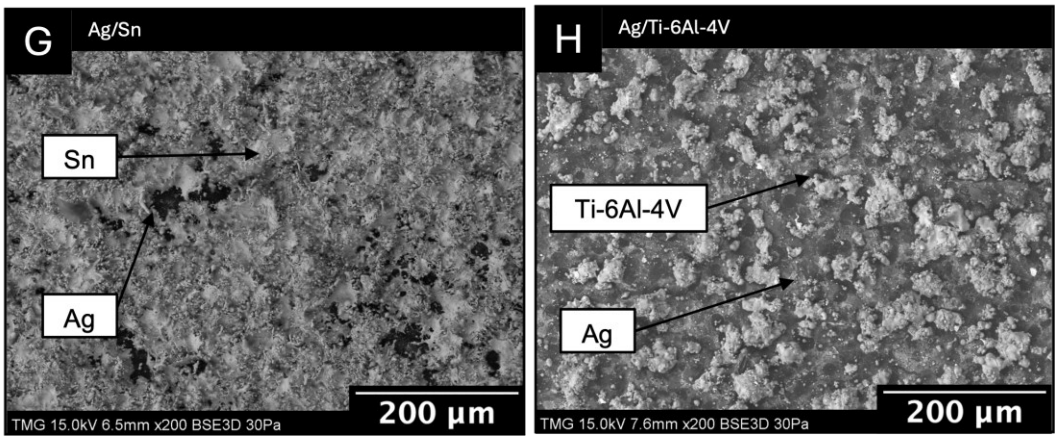


*Figure 5: SEM top surface images of the APS sprayed electroless plated coatings. Where A) No plating + Sn, B) No plating + Ti-6Al-4V, C) Ni + Sn, D) Ni + Ti-6Al-4V, E) Cu + Sn, F) Cu + Ti-6Al-4V, G) Ag + Sn & H) Ag + Ti-6Al-4V*

The surface of the electroless-plated Ni sample with Ti-6Al-4V coating is displayed in Figure 6. The figure highlights two regions: one with surface cracks (Figure 6a) and another with microcracks (Figure 6c) distributed across the sample's surface. These defects vary in length and orientation, disrupting the cohesion of the coating at a macroscale but also at a microscale. The microscopic fractures depicted in Figure 6c divide the particle splat, resulting in cracks in the coating.

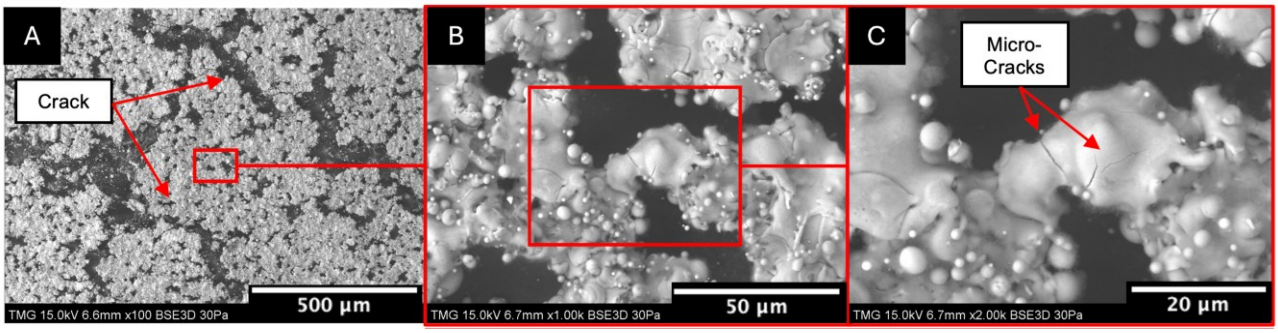


*Figure 6: SEM top surface image of the Ti-6Al-4V APS sprayed coating on the Ni electroless plated sample at several magnifications. Where A) 100x magnification, B) 1000x magnification & C) 2000x magnification*

The surface of the coatings was also characterized using micro-CT scanning, as shown in Figure 7, in order to obtain a better representation of the coating density, as well as presence of pores or voids. In the top surface images of the APS sprayed coatings, the lighter areas represent the substrate material, while the darker areas represent the deposited coating. The brightness observed in certain images of Ti-6Al-4V thermally sprayed coatings indicates the low density of the deposited layer on the electroless-plated interlayer (bond coat), which fully covers the substrate. The variations in brightness can be attributed to the

microstructures of the Ti-6Al-4V layer, which may display porosity or incomplete splat formation, leading to regions of diminished coating density (i.e. the brighter regions). It can be observed that the plating material between the substrate and the coating, as well as the coating material significantly affected the coating's density. When the substrate material was plated with Ni, there were fewer pores, and therefore observably better build-up of the coating with improved adhesion of the sprayed particles. In addition, the thermal sprayed Sn coatings exhibit the lowest number of pores compared to all other samples. In cases where the thermal spraying was done directly on the non-plated substrate material, the Ti-6Al-4V showed the least amount of coating deposition. Overall, the Sn coatings were significantly denser than the Ti-6Al-4V coatings.

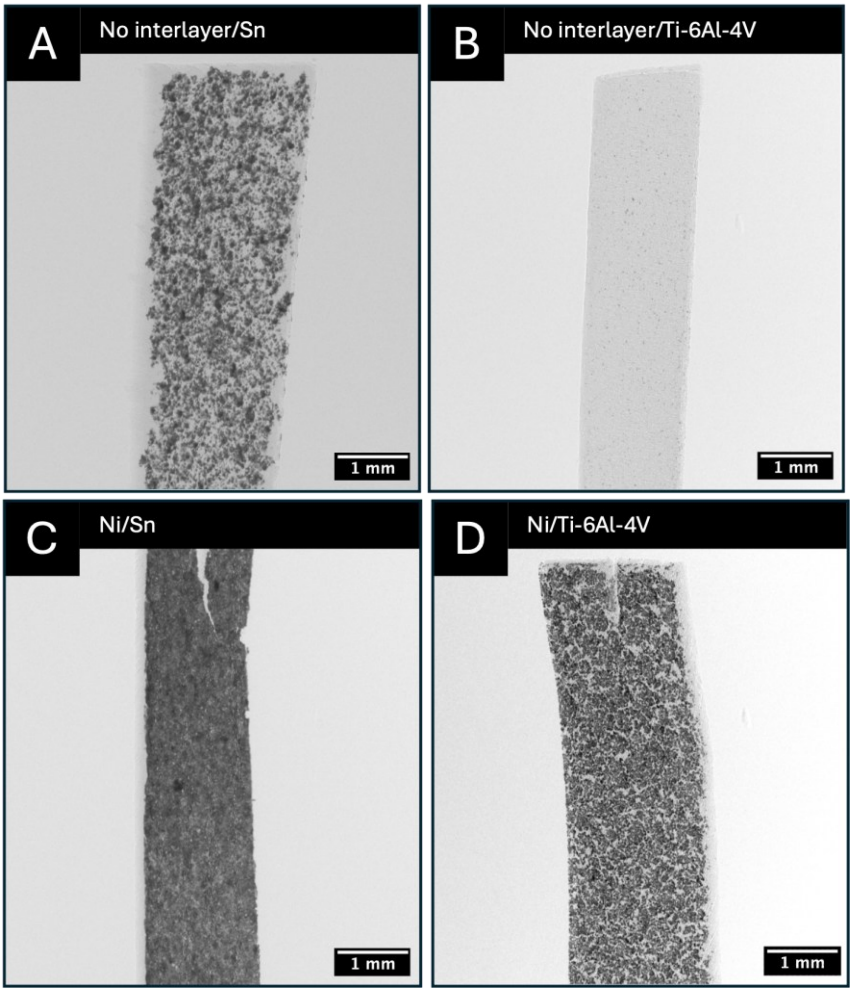

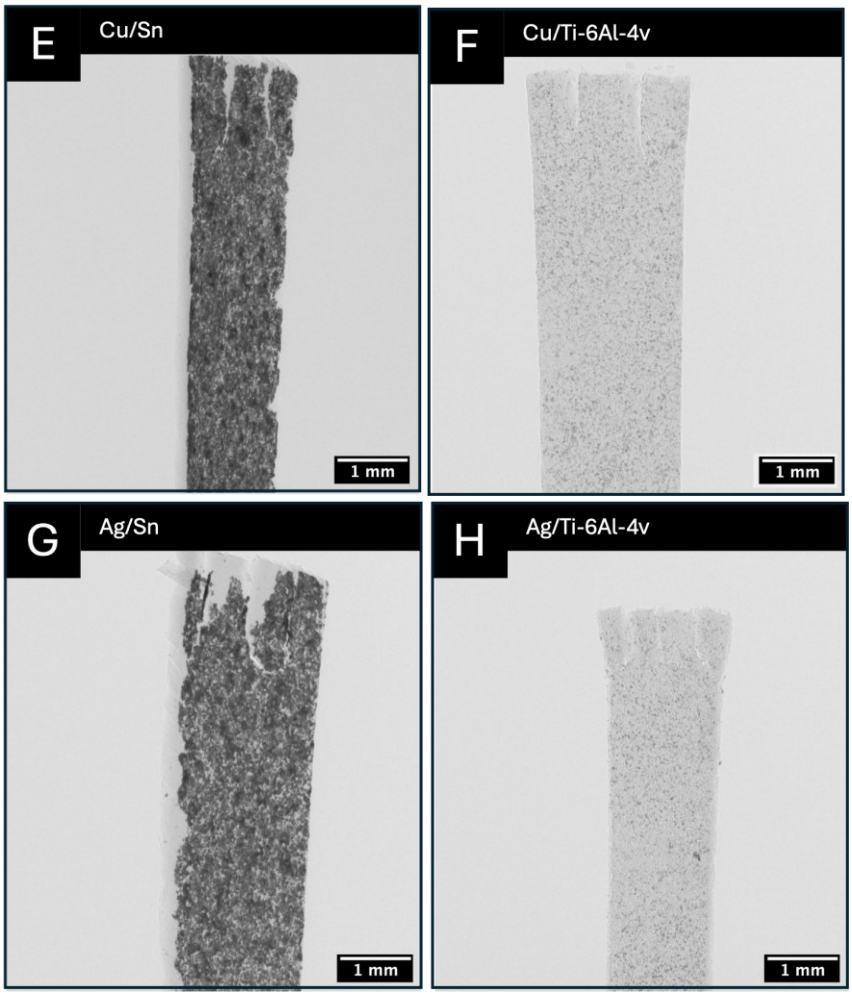


*Figure 7: Micro-CT scans of the APS sprayed electroless plated samples. Where A) No plating + Sn, B) No plating + Ti-6Al-4V, C) Ni + Sn, D) Ni + Ti-6Al-4V, E) Cu + Sn, F) Cu + Ti-6Al-4V, G) Ag + Sn & H) Ag + Ti-6Al-4V*

The surface roughness (Sa) was assessed using confocal microscopy, and the resulting data are illustrated in Figure 8, complete with error bars to represent variability. This figure displays the results for the CF-LMPAEK, electroplated coatings, as well as the Sn and Ti-6Al-4V coatings. The uncoated CFRP substrate exhibited a low surface roughness of approximately 1 µm. Following electroless plating, a substantial increase in roughness was noted, particularly for the copper and silver coatings, which both exhibited roughness values in the range of 6 to 7 µm. Nickel plating resulted in a reduced roughness of around 1 µm, which was even lower than that of the uncoated CFRP. After the Atmospheric Plasma Spraying (APS) deposition, a further escalation in surface roughness was observed across all samples. The Sn-coated specimens showed a roughness range of approximately 6 to 9 µm, with silver-coated samples presenting a slightly elevated average roughness compared to those coated with nickel and copper. The Ti-6Al-4V coatings displayed the highest roughness, reaching values of about 10 to 12 µm, with the nickel interlayer

contributing to the most significant increase in average roughness. This finding suggests that the thermal spray process introduces additional surface irregularities, likely due to splat formation and coating buildup.

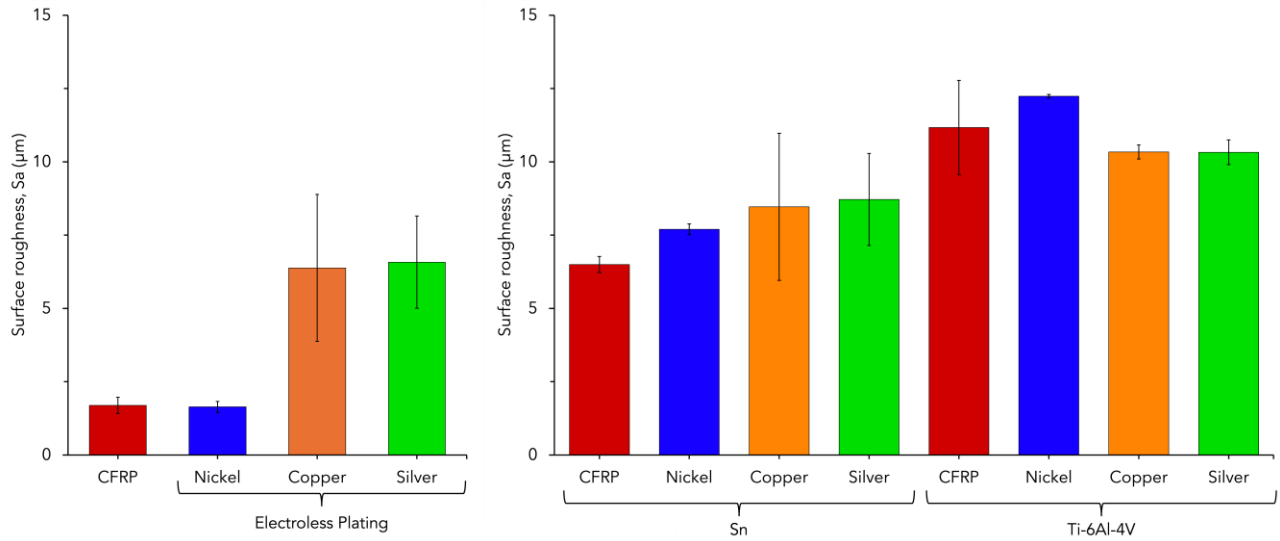


*Figure 8: Surface roughness of the electroless plated samples and the APS sprayed samples*

### 3.4.1.2. Cross-sectional Characterization

The images in Figure 9 show the cross-sections of the Ti-6Al-4V and Sn coatings applied on top of the electroless plated interlayer film (Ni, Cu, or Ag) using the APS process. The Sn deposits result in a more uniform coating with very few spherical particles, while the Ti-6Al-4V coatings produce a coating with spherical particles. Additionally, the deposition of the Ti-6Al-4V coating leads to significant deformation of the polymer, causing the fiber orientation to deviate from its normal alignment. On the other hand, the polymer matrix and fibre orientation show no significant deformation with Sn coatings.

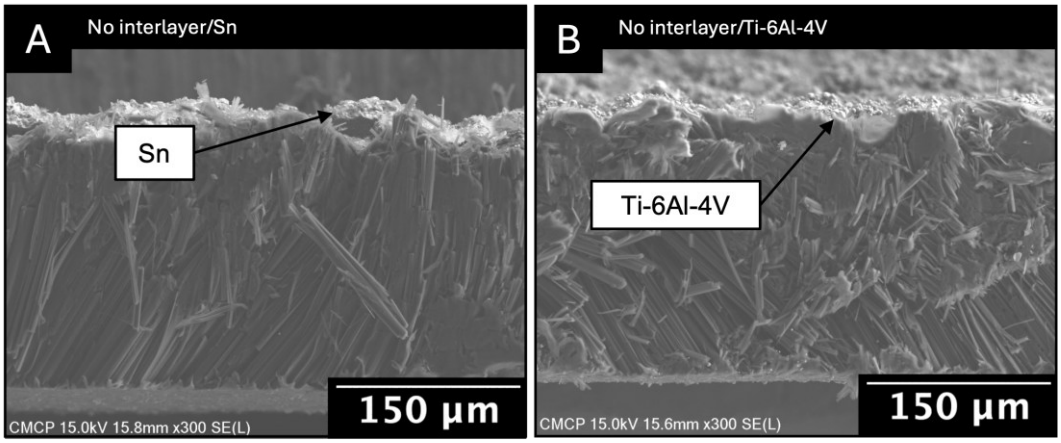

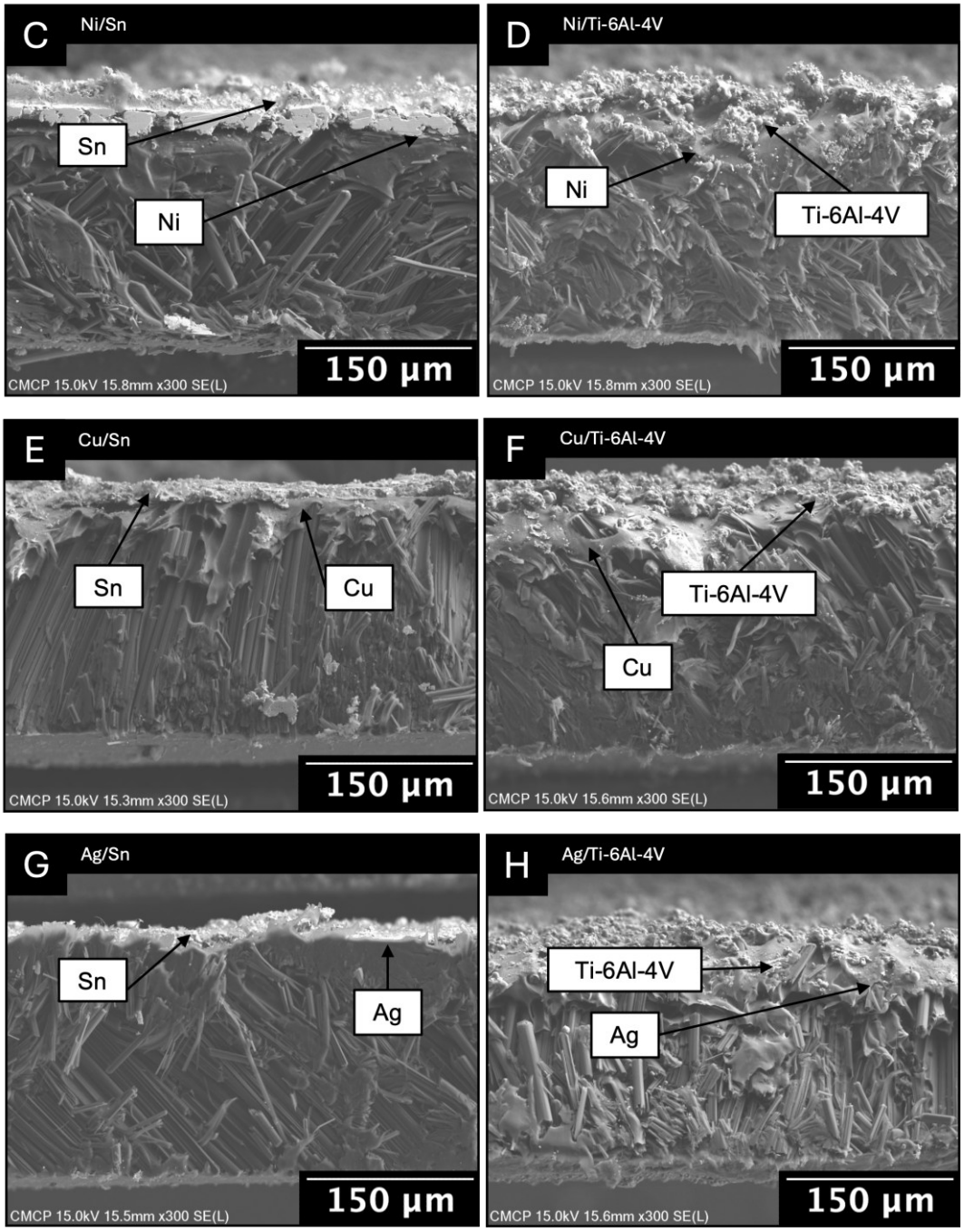


*Figure 9: FESEM cross-sectional images of the APS sprayed electroless plated samples. Where A) No plating + Sn, B) No plating + Ti-6Al-4V, C) Ni + Sn, D) Ni + Ti-6Al-4V, E) Cu + Sn, F) Cu + Ti-6Al-4V, G) Ag + Sn & H) Ag + Ti-6Al-4V*

The thickness of the coatings was obtained using the high-magnification FESEM images and image analysis software (ImageJ) where the results are summarized in Table 5. From the cross-sectional images of the samples in Figure 9, it can be observed that the deposited coatings onto the substrate demonstrate some

irregularity, as evidenced by variations in coating thickness across the cross-sections. To account for this, the mean thickness values were obtained from the averages of multiple cross-sectional measurements across the samples. The associated error ranges (standard deviations) between the measurements have been included to provide a more comprehensive representation of the thickness. These error ranges represent the variability caused by the irregular morphology of the coatings. Despite the observed irregularities, the measured thickness values remain consistent with the deposition trends observed for each material and plating condition. The results in Table 5 are further clarified below in terms of the mean thickness of the interlayer, the mean thickness of the thermal spray coating, and the overall mean total thickness.

The electroless plating interlayer thickness onto the substrate material varied among the different metals, with nickel (Ni) plating yielding on average the highest thickness (9.71 µm), followed by silver (Ag) at 6.44 µm and copper (Cu) at 5.90 µm. These variations can be attributed to differences in deposition rates and plating solution properties. Furthermore, it can be observed that the thickness of the thermal spray coating is highly dependent on the material of the interlayer sprayed on. Samples with Ni interlayer exhibited the thickest thermal spray coatings for both Sn (15.37 µm) and Ti-6Al-4V (12.38 µm). The coatings sprayed on Ag and Cu interlayers showed comparable, yet slightly thinner, results. Samples without any electroless plating had the thinnest thermal spray coatings, with Ti-6Al-4V exhibiting minimal deposition. Finally, considering both the thickness of the interlayer and thermal spray coating thicknesses, the Ni-plated samples exhibited the greatest overall thickness, reaching 25.08 µm for Sn coatings and 22.09 µm for Ti-6Al-4V coatings. Ag- and Cu-plated samples demonstrated intermediate total thickness values, while non-plated samples showed the lowest total thickness due to the absence of an interlayer. This detailed breakdown emphasises the relationship between interlayer type and the resulting thermal spray and total thickness values, highlighting Ni as the most effective plating material for achieving thick and uniform coatings.

*Table 5: Average thickness of the APS sprayed electroless plated coatings on CF-LMPAEK samples*

| | Electroless Plating Thickness (µm) ± SD | Sn Coating Thickness (µm) ± SD | Total Sn Coating Thickness (µm) ± SD | Ti-6Al-4V Coating Thickness (µm) ± SD | Total Ti-6Al-4V Coating Thickness (µm) ± SD |
|---|---|---|---|---|---|
| No Interlayer | - | 10.89 ± 0.81 | 10.89 ± 0.81 | 7.36 ± 1.20 | 7.36 ± 1.20 |
| Ni Interlayer | 9.71 ± 0.25 | 15.37 ± 0.82 | 25.08 ± 0.85 | 12.38 ± 1.03 | 22.09 ± 0.24 |
| Cu Interlayer | 5.90 ± 0.42 | 10.69 ± 0.99 | 16.59 ± 1.07 | 10.57 ± 1.26 | 16.47 ± 0.34 |
| Ag Interlayer | 6.44 ± 0.90 | 9.7 ± 1.19 | 16.14 ± 1.49 | 10.46 ± 1.26 | 16.90 ± 0.88 |

Figure 10 presents EDS elemental mapping of different electroless plated interlayers on CF-LMPAEK substrates prior to thermal spraying. In the Ni-plated sample (A), the Ni elemental distribution (blue) appears as a distinct and continuous interlayer at the interface. In the Cu-plated sample (B), the Cu elemental map (orange) reveals a well-defined plating layer, though some diffusion into the surrounding regions is visible. In contrast, the Ag-plated sample (C) shows a more dispersed Ag signal, making it difficult to clearly identify a continuous plating layer. Additionally, the presence of contaminants can be observed in the plated samples, likely resulting from residual materials in the electroplating bath and the various plating solutions used.

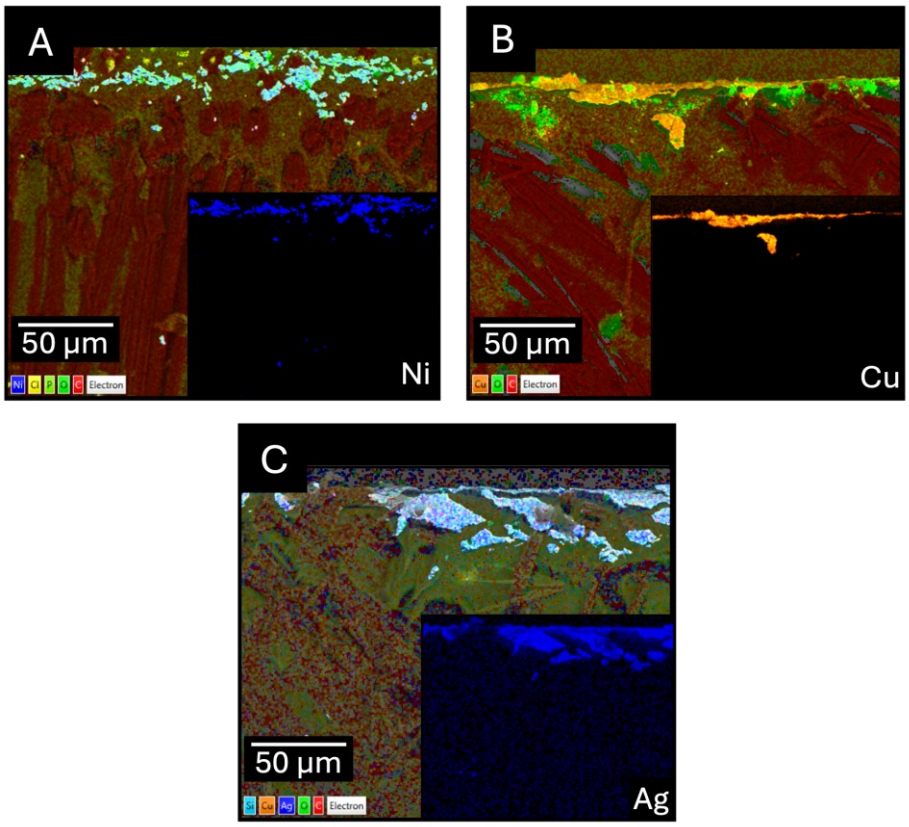


*Figure 10: EDS mapping of cross-sectional electroless plated CF-LMPAEK samples*

In addition, the composition analysis of the thermally sprayed coatings is illustrated in Figure 11. The EDS results confirm that the plating materials (Ni, Cu, and Ag) adhered uniformly and served as an interlayer for coating done using APS, facilitating the formation of an adherent coating. However, the absence of an EDS map for the Ag interlayers in panel G can be attributed to the thermal sprayed coating, since the Ag is visible in Figure 10. The thermal spray coating effectively obscures the interlayer, rendering the elements

undetectable under EDS mapping. In addition, the analysis of the Sn samples revealed the presence of trace contaminants, including Ti, Al, and V. These contaminants are likely attributable to the sequence in which the coatings were applied, with the Ti-6Al-4V samples being coated prior to the Sn coating. The presence of these contaminants, as shown in Figure 11 (b) and Figure 11 (f), may be attributed to residual material present in the feeder and/or the feeding line.

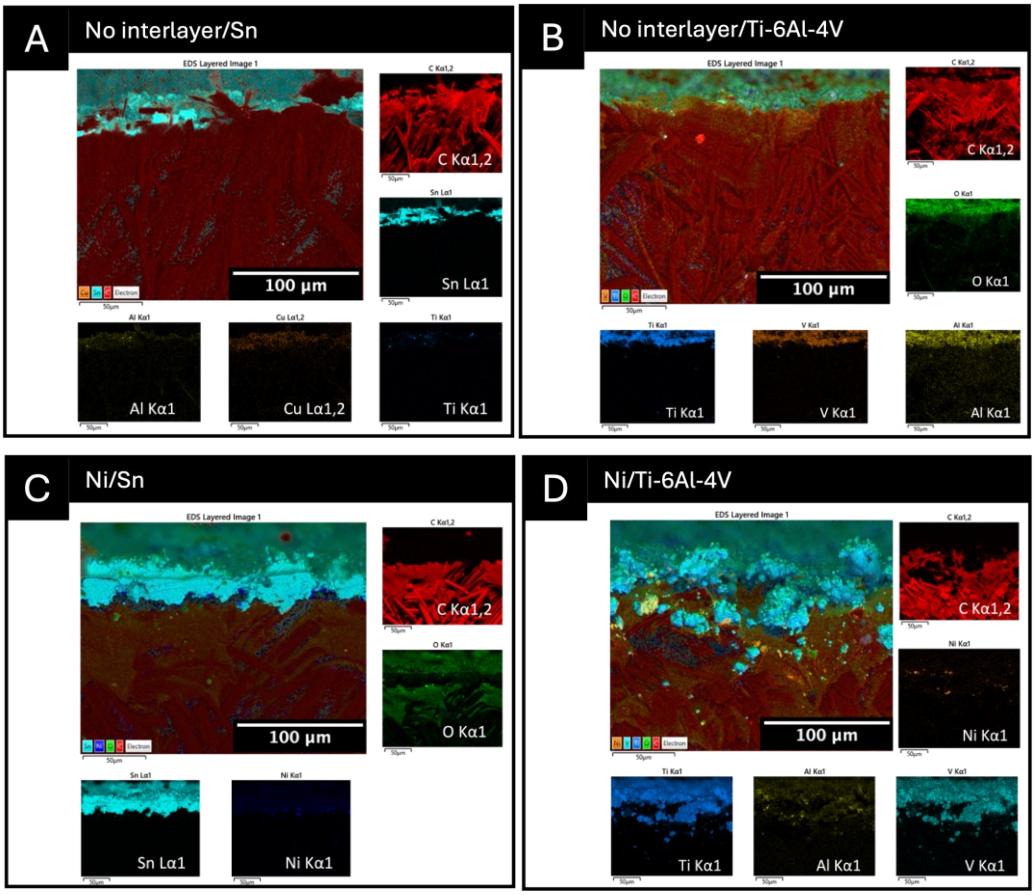

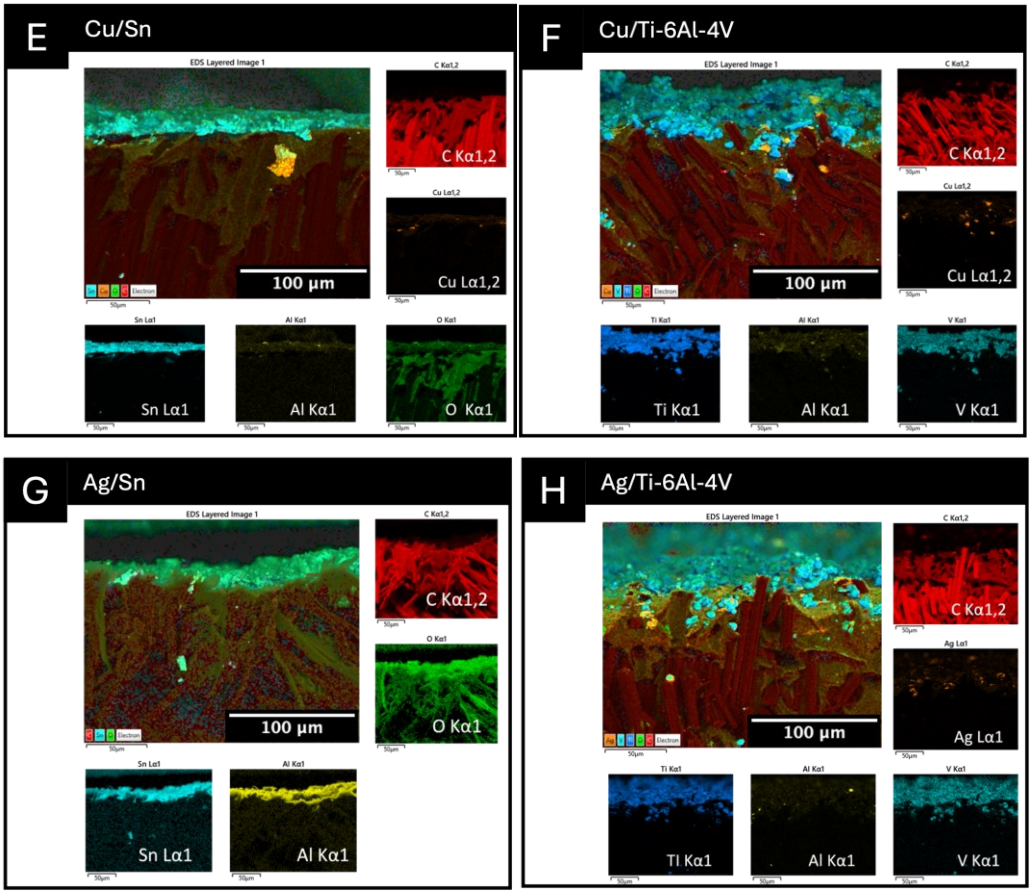


*Figure 11: EDS mapping of the cross-sectional images of the APS sprayed electroless plated samples. Where A) No plating + Sn, B) No plating + Ti-6Al-4V, C) Ni + Sn, D) Ni + Ti-6Al-4V, E) Cu + Sn, F) Cu + Ti-6Al-4V, G) Ag + Sn & H) Ag + Ti-6Al-4V*

### 3.4.1.3. Thermal Characterization

The thermal resistance of the samples in this study was measured using the Nano Test TIMA 5 thermal interface material analyzer and is shown in Figure 12. The results indicate that the Sn samples demonstrated lower thermal resistance compared to the Ti-6Al-4V samples. Among the different combinations of plating and coatings, Ni displayed the highest thermal resistance when paired with Ti-6Al-4V, in comparison to Cu and Ag interlayers. The CFRP sample without any plating or coating showed the minimum thermal resistance, while the Ni-plated samples with the Ti-6Al-4V coating exhibited the maximum thermal resistance.

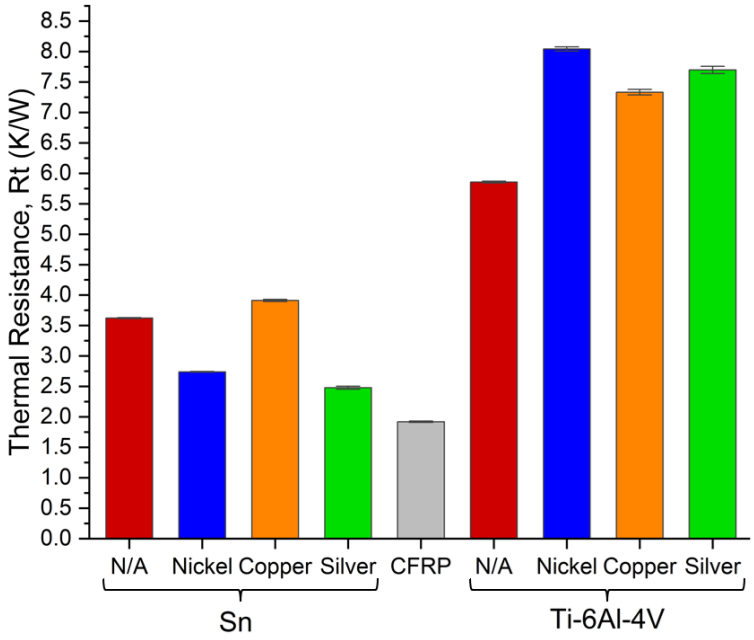


*Figure 12: Thermal resistance of the APS sprayed electroless plated samples*

### 3.4.2. HVAF

Figure 13 illustrates the outcome of the HVAF process when attempting to coat the substrate samples with Ti-6Al-4V following the initial pass with the i7™ internal diameter thermal spray gun. The samples, which were attached as shown on Figure 4, were exposed to maximum particle velocities of 800 m/s [55], resulting in their destruction as seen on Figure 13, and making them unsuitable for further characterization.

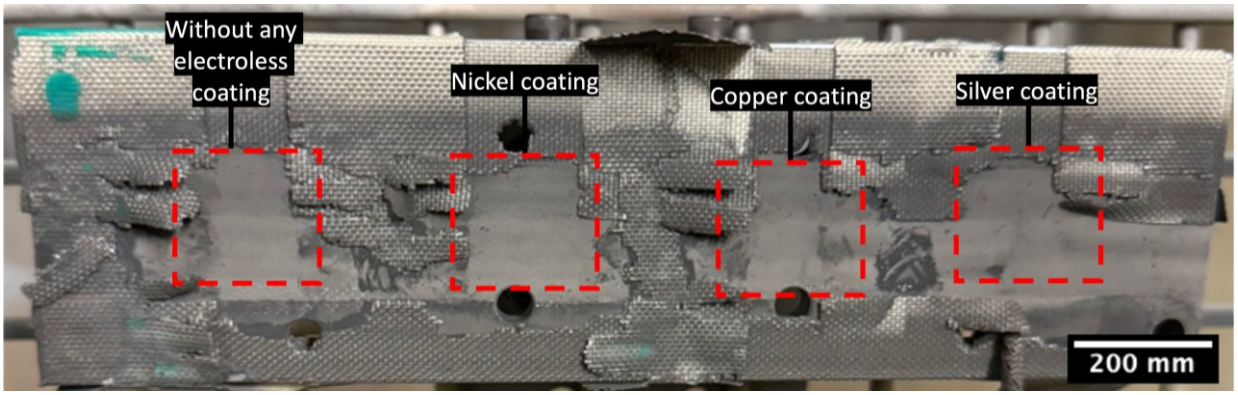


*Figure 13: Image of samples taken after HVAF spraying*

## 3.5. Discussion

The thickness of the electroplated interlayer ranges between 5 and 10 µm depending on the metal being

deposited (i.e. Ni, Cu and Ag). The thickness of the plating is closely related to the deposition rate, which can vary based on solution pH, temperature, and bath loading [63]. In this study, the variation in coating thickness can be attributed to differences in pH levels among the different plating solutions, as both temperature and bath loading were maintained at constant levels. The pH values presented in Table 6 are speculative and derived from literature-based procedures for the electroless deposition of these metals. Although these values generally reflect typical conditions reported for the deposition of Ni, Cu, and Ag, they were not directly measured during this study. The observed values suggest a correlation between coating thickness and solution pH, indicating that higher pH levels are associated with thinner coatings. In addition, the variations in interlayer thickness are influenced not only by the pH of the plating baths but also by the inherent properties of the metals being deposited, their specific deposition kinetics, and their surface energy [64]. Surface energy plays a critical role in determining the interaction between the substrate and the deposited metal, as well as the wetting behavior of the plating solution [65]. For instance, nickel, with its higher surface energy (as shown in Table 7), promotes better adhesion and more uniform deposition compared to copper or silver, which have lower surface energies. These factors, in combination with pH, plating kinetics, and bath composition, contribute to the observed differences in interlayer thickness.

*Table 6: pH level of electroless plating solutions*

| | Nickel solution | Copper solution | Silver solution |
|---|---|---|---|
| pH level | 4.5-5.0 [66] | 12.5 [67] | 7.5 [68] |

After the electroless plating, the APS process was used to metalize the CFRP. The combination of different plating and coating materials resulted in different coating microstructure, which are detailed in section 3. The process parameters were optimized to minimize heat transfer to the baseline polymer matrix thus minimizing the risk of substrate degradation. Specifically, the injection angle was set to 20 degrees to reduce the exposure time of the powder particles in the plasma. The results of the micro-CT images (Figure 7), along with the cross-sectional analysis of the samples (Figure 9 and Figure 11), have shown that the Sn coating exhibits a uniformly dense microstructure, while the Ti-6Al-4V coating shows agglomeration with more spherical particles. However, for both the Ti-6Al-4V and Sn coatings on the plated samples, those with a Ni interlayer exhibited more uniform and homogeneous coatings with fewer pores compared to those with Cu or Ag plating. The results observed for the APS process in this study indicate that a significant portion of the particles achieve a molten state. However, the formation of spherical particles in the Ti-6Al-4V coatings suggests that certain particles either impact the substrate with insufficient kinetic energy or form secondary droplets during splatting. The presence of sub-5 μm spherical features on the surface (as shown in Figure 6) indicates that either fine feedstock particles underwent

complete melting but impacted with low velocity—limiting their spread—or larger molten particles splatted upon impact, generating peripheral droplets that redeposited at low velocity. These mechanisms align with prior observations in APS coatings where variations in particle size and velocity affect splat morphology [69]. Further analysis of in-flight particle velocities and temperature distributions would provide additional insights into these deposition dynamics. This phenomenon is influenced by the material properties of the sprayed particles as well as the interlayer materials, which are tabulated in Table 7 [70]. Notably, the differences in thermal conductivity and surface characteristics of interlayer materials (e.g., Ni, Cu, Ag) could result in varying amounts of splashing and particle morphology. For instance, interlayers with superior thermal conductivity, such as those composed of Cu and Ag, have been shown to facilitate more rapid cooling of the impacting particles, thereby enhancing the probability of solidification splashing [70]. When the thermal conductivity of the plating interlayer is high, the heat from the impacting sprayed particles is rapidly transferred through the interlayer to the CFRP, which can lead to the thermal degradation of the polymer matrix. Lower interlayer temperatures allow less time for the sprayed particles to form uniform splats, resulting in fewer disc splats and more spherical particles on the sample surface due to rapid cooling [71]. This can lead to decreased coating density, particularly observed in the Cu and Ag plating samples, as seen in Figure 5 and Figure 7. In the case of Ti-6Al-4V coatings, the high particle temperature and high thermal conductivity of the Cu and Ag-plating result in significantly less dense coatings due to lower adhesion of the sprayed particles on their surfaces and the thermal degradation of the CFRP substrate. On the other hand, Ni has the lowest thermal conductivity, acting as a better thermal insulator and conducting less heat energy to the substrate material. The Ni plating absorbs heat from the impact of spraying particles within the plating layer, transferring it less rapidly to the CFRP than other plating materials. This protects the CFRP from the heat and provides an improved bonding surface for initial particle adhesion during the first spray pass. The low thermal conductivity of the Ni-plating interlayer prevents the splats from shrinking upon impact, ensuring a better adhesion and build-up of the coating [72]. This phenomenon explains why the Ni-plated samples in Figure 5 and Figure 7 facilitate the formation of thicker and less porous coatings, particularly when Sn is sprayed. The lower temperature of the impacting Sn particles, in contrast to those of Ti-6Al-4V, helps maintain the integrity of the matrix material. This effect can be observed more clearly in the EDS maps obtained from the cross-section in Figure 11, highlighting a noticeably greater deposition thickness of Sn and Ti-6Al-4V elements over the Ni plating. In instances where no plating was used, and spraying was done directly on the CFRP, the resulting coating thickness was significantly reduced for the Ti-6Al-4V coating. Additionally, it is important to consider the thermal expansion coefficient of the plated material (Table 7), as it indicates how the material expands when heated. The difference in thermal expansion coefficients between the electroplated interlayer and the CFRP substrate may contribute to thermal stresses at the interface during heating. While CFRP generally

has a higher coefficient of thermal expansion (CTE) than the metal interlayers, the mismatch in expansion can still influence coating adhesion and introduce interfacial stresses, particularly for Cu and Ag, which have higher CTEs than Ni. Since the fibers are oriented in the normal direction and the plating is applied on top, this could displace the fibers, leading to misalignment in the normal direction. As a result, this misalignment may cause increased warping of the polymer in the samples, ultimately reducing the adhesion of the sprayed particles to the surface. This issue was particularly evident when examining the cross-section of the samples in Figure 9, especially in the case of the Ti-6Al-4V coated samples.

*Table 7: Relevant properties of materials explored in this study*

| | Nickel | Copper | Silver | Ti-6Al-4V | Sn | CF-LMPAEK |
|---|---|---|---|---|---|---|
| Melting Point (ºC) | 1453 [73] | 1084 [73] | 961 [73] | 1604-1660 [73] | 231.93 [73] | - |
| Surface energy ($J/m^2$) | 2.34 [33] | 1.65 [74] | 1.065-1.54 [75] | 0.06175 [76] | 0.7 [77] | - |
| Thermal Conductivity (W/m·K) | 91 [78] | 391 [79] | 429 [79] | 6.7 [30] | 66 [79] | 18-22 |
| Thermal Expansion Coefficient ($10^{-6}$ m/mºC) | 13.4 [80] | 17.6 [79] | 19.8 [79] | 8.6 [30] | 23 [79] | - |
| Heat of fusion (kJ/mol) | 17.2 [81] | 13.1 [81] | 11.3 [81] | 127.57 [82] | 7 [81] | - |
| Specific Heat Capacity (J/kg·K) | 502.42 [83] | 376.81 [83] | 238.65 [83] | 526.3 [84] | 217.71 [83] | - |

Furthermore, as shown in Table 7, Sn exhibits a significantly lower melting point, heat of fusion, and specific heat capacities compared to Ti-6Al-4V. These factors notably impact the thermal energy stored in the particles during the deposition process. The disparities indicate that Ti-6Al-4V particles necessitate considerably more thermal energy for melting and maintaining a liquid state. Moreover, a higher melting point suggests that a larger amount of thermal energy may be stored and subsequently released onto the substrate material during deposition. Consequently, Ti-6Al-4V has the potential to release a greater amount of heat during deposition, which could result in substrate deformation and the burning of polymer materials, thereby compromising the integrity of the matrix. This phenomenon was notably observed when the Ti-6Al-4V coating was directly applied to the CFRP surface without any plating, as depicted in Figure 5(b). In contrast, the higher concentration of molten particles in the case of Sn coatings indicates that there is less thermal energy stored within the material, which is released into the substrate as the particles solidify and cool during deposition [85]. This thermal behavior aids in the formation of more uniform, disk-shaped splats on the surface and promotes effective coating build-up. Overall, the disparities in thermal properties correlate well with the observed splat morphologies in Figure 5 where Sn forms more uniform disk splats due to its lower energy requirements for melting and spreading, while Ti-6Al-4V exhibits a higher proportion of partially melted particles and spherical morphologies due to its higher energy demands.

The interaction between the molten thermal spray splats and the solid electroplated interlayer, particularly wettability, also play a significant role in the coating morphology. Wettability is defined as the degree to which molten particles spread and adhere to the interlayer surface [86]. This phenomenon is influenced by surface energy and geometric structures [87]. Improved wetting of the substrate by the splat has been shown to decrease splat thickness and increase splat radius, which enhances splat-substrate adhesive bonding [88]. For instance, Sn, having high surface energy, is expected to exhibit better wetting behavior compared to Ti-6Al-4V [89]. This difference could help explain the variations in coating uniformity and adhesion observed between the Sn and Ti-6Al-4V coatings. Additionally, the surface energy, chemical compatibility, and roughness of the interlayer material also significantly influence the wetting dynamics [87]. For example, the Ni interlayer, with its higher surface energy, may enhance wetting and splat formation compared to Cu or Ag interlayers, contributing to the more uniform coatings observed with Ni. While the initial observations made from Figure 5 provide an overview of the surface morphology of the coatings, they lack sufficient detail for a comprehensive analysis of the particles. Further investigation is necessary to obtain a single flat projection on the sample (i.e., using a very low powder feed) to better analyze the influence of interlayer materials on splashing behavior.

The difference between the different coating's microstructure and the influence of material properties (Table 7) are well correlated with the surface roughness results shown in Figure 8. Surface roughness significantly influences splat adhesion and coating performance. The increase in roughness following electroless plating can suggests an enhancement in mechanical interlocking, which can be beneficial for APS deposition. However, while nickel-coated samples exhibited lower initial roughness compared to copper and silver, this did not negatively impact deposition. On the contrary, as seen in Table 5, nickel coatings resulted in higher deposited thickness for both Sn and Ti-6Al-4V, suggesting that factors beyond roughness, such as surface chemistry or wettability, may have contributed to improved adhesion. The APS process further increased surface roughness, particularly for Ti-6Al-4V coatings. This trend suggests that Ti-6Al-4V deposition leads to more pronounced splat stacking and surface irregularities compared to Sn coatings, which exhibited a more uniform roughness distribution. In other words, Sn coatings exhibited lower overall surface roughness compared to the Ti-6Al-4V coatings. The observations regarding surface roughness have a significant impact on the thermal resistance values presented in Figure 12. Variations in the morphology of the coated samples, stemming from differences in splat formation and the distinct material properties, specifically the thermal conductivity of both the interlayer and the coating materials, play a critical role in influencing thermal resistance. For example, the Sn coatings, which exhibit a smoother and more uniform splat morphology, demonstrate lower thermal resistance and superior performance

compared to the Ti-6Al-4V coatings. This improved performance is attributed to the effective spreading and cohesion of Sn splats, which minimize voids and roughness, thereby enhancing thermal conductivity. In contrast, the irregular and partially melted splats found in the Ti-6Al-4V coatings result in increased porosity and roughness, leading to diminished thermal performance. On the other hand, the CFRP substrate (before plating and coating) exhibited the lowest thermal resistance, approximately 2.2 K/W. This low value is likely due to the high thermal conductivity of the carbon fiber combined with the polymer matrix, which, in the absence of a coating, does not contribute additional resistance to the measurements. Consequently, the interplay between thermal properties, deposition conditions, and microstructural characteristics directly correlates with the thermal resistance values observed in this study.

Overall, the addition of the interlayer improved the coating compared to the non-plated samples in terms of coating thickness and uniformity. This is especially evident for the nickel interlayer, where both the Sn and Ti-6Al-4V coatings were more uniform than the other sprayed samples in Figure 7 (c) and (d), respectively. This can likely be attributed to the material properties of the nickel-plated interlayer (see Table 7) compared to the other plating materials and the increased coating build-up. The schematic on Figure 14 summarizes the effectiveness of the material used and the interlayer process before the thermal spray coating is applied.

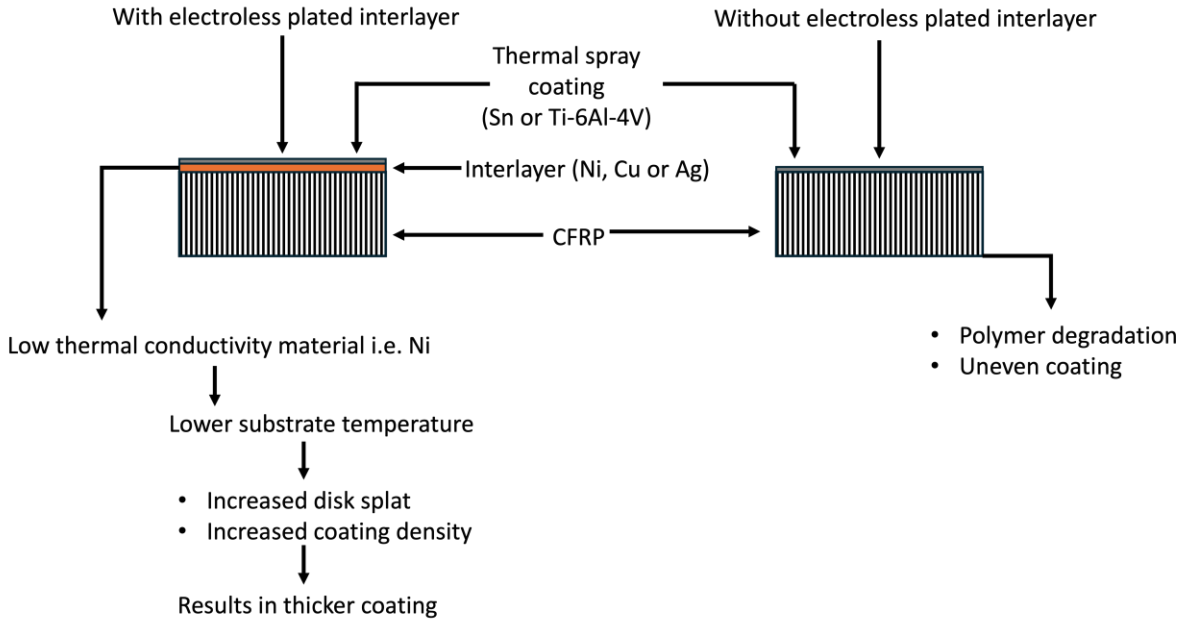


*Figure 14: Schematic of improvements provided by the thermal spraying of coatings on electroless plated CFRP samples*

It should be noted that the HVAF method was also investigated for depositing Sn and Ti-6Al-4V coatings

on the electroplated substrates. However, this approach proved to be unsuccessful when using the same substrate material and electroplated interlayer as the APS process. The higher velocity of the particles during the HVAF process, which can reach up to 800 m/s [90], resulted in a significant amount of kinetic energy transfer upon impact, ultimately causing damage to the substrate as depicted in Figure 13. For future development employing this thermal spray method, adjusting the parameters related to the formation of the electroplated layer could contribute to achieving deposition, thereby aiding in safeguarding the substrate material from damage caused by the high-velocity impact of the particles.

## 3.6. Conclusion

Ti-6Al-4V and pure Sn were deposited onto CF-LMPAEK substrates plated with Ni, Ag, and Cu using the APS and HVAF processes, aiming to metallize CFRPs. The HVAF process resulted in substrate degradation, which limits its effectiveness for coating single layers of CFRP. In contrast, the deposition of Sn through APS was accomplished successfully, yielding smoother coatings, whereas the spraying of Ti-6Al-4V particles caused damage to the CF-LMPAEK substrate. The characteristics of the electroless plating materials, particularly the melting temperature, thermal conductivity, and thermal expansion values, significantly influence the outcomes of the sprayed coatings. Both Sn and Ti-6Al-4V demonstrated greater deposition efficiency (i.e. thickness) and improved coating performance with Ni plating. Overall, the Sn coatings exhibited lower thermal resistance compared to those of Ti-6Al-4V. For Sn coatings, the Ni interlayer resulted in the lowest overall thermal resistance among the materials tested. In contrast, Cu and Ag interlayers led to more porous coatings with higher thermal resistance. Overall, this study identified that Ni-electroplated CFRP samples coated with Sn via the APS process exhibited the most favorable coating characteristics, making this combination the optimal choice of plating and coating materials for the APS thermal spray process. Future research should explore the impact of interlayer properties on splat morphology and adhesion strength further.

# Chapter
# 4. Conclusion and Future Direction

This chapter concludes the proposed methodology for the development for metalized carbon fiber in aligned in the normal direction with the focus on surface deposition, thermal and tribological properties.

## 4.1. Conclusion

The research presented in this thesis has advanced the understanding and development of MMCs with normal orientation and the application of thermally sprayed metallic coatings onto CFRPs. It has also provided valuable insights into their design, fabrication, and potential applications. The integration of these materials holds great promise for improving the performance of structural components in various industries, including aerospace, automotive and energy.

The application of thermally sprayed metallic coatings on polymer-reinforced carbon fiber composites was explored in detail, demonstrating the feasibility of using coatings to enhance the surface properties of composite materials. The performance of the sprayed coatings is strongly influenced by the properties of the electroless plating materials, particularly their melting temperature, thermal conductivity, and thermal expansion characteristics. Based on this study, the optimal combination of plating, coating, and spraying is achieved using Ni electroless plating with tin applied through the APS thermal spray process. Challenges related to the thermal compatibility between the polymer matrix and metallic coatings were successfully addressed, paving the way for further exploration of these composite systems in high-temperature or aggressive environmental applications. The resulting coatings exhibited superior adhesion and durability, thereby enhancing the versatility and suitability of polymer-reinforced carbon fibre composites for a broader range of applications.

The development and characterisation of vertically aligned metallized carbon fibre composites represents a promising avenue of research for the creation of lightweight, high-strength, and thermally stable materials. Furthermore, they provide practical pathways for enhancing the performance of composite materials. This study serves as a foundation for ongoing investigation and optimisation of these materials.

## 4.2. Future Work

While the findings of this research provide a solid foundation, there are several avenues for future work that could further enhance the understanding and application of normal orientation thermally sprayed metallic coatings on PMCs.

Further studies on the environmental performance of normal orientation PMCs would also be valuable, particularly in terms of their resistance to high-temperature oxidation and degradation in aggressive

atmospheres. The incorporation of novel matrix materials, such as bio-based resins or matrix materials with improved high-temperature stability, could be explored to enhance the environmental sustainability of these composite systems [91]. Additionally, the use of natural fibers, such as flax and hemp, instead of synthetic fibers can be explored in the normal orientation as a variation and permutation of the composite design [92]. Furthermore, a deeper understanding of the effect of processing variables on the microstructure and properties of the composites, including grain structure, and phase transformation, will help to optimize their performance for demanding applications.

In terms of thermally sprayed metallic coatings, future research could also investigate the use of novel coating materials, such as ceramic or carbide-based coatings, to enhance wear and oxidation resistance at elevated temperatures [93]. Furthermore, hybrid coatings that combine multiple metallic and non-metallic phases could be studied to achieve a combination of mechanical, electrical, and thermal properties tailored to specific applications [94].

Future work could also incorporate advanced modeling techniques to predict the behavior and performance of composite materials and coatings. Computational tools, such as finite element analysis (FEA) or machine learning algorithms, could be utilized to simulate the mechanical, thermal, and environmental performance of the materials, helping to accelerate the design process and identify optimal material configurations [95]. Integration of experimental data with predictive models could provide a more comprehensive understanding of material behavior, leading to more efficient design and development of next-generation composites and coatings [96].

In conclusion, the findings of this research provide a strong basis for further exploration of MMCs and thermally sprayed coatings, which have the potential to transform material systems for a range of high-performance applications. The ongoing advancement of these technologies will facilitate the development of more sustainable, efficient, and resilient materials for future applications.

# 5. References


[1] F. Addou *et al.*, “Metallization of carbon fiber reinforced polymers: Chemical kinetics, adhesion, and properties,” *Surface and Coatings Technology*, vol. 308, pp. 62–69, Dec. 2016, doi: 10.1016/j.surfcoat.2016.06.098.

[2] A. C. Liberati *et al.*, “Effect of Carbon Fiber Orientation when Cold Spraying Metallic Powders onto Carbon Fiber Reinforced Polymers,” Accessed: Jun. 20, 2024. [Online]. Available: https://dx.doi.org/10.31399/asm.cp.itsc2023p0280

[3] T. W. Clyne and D. Hull, *An Introduction to Composite Materials*. Cambridge University Press, 2019.

[4] W. D. C. Jr and D. G. Rethwisch, *Materials Science and Engineering: An Introduction*. John Wiley & Sons, 2020.

[5] B. Harris and Institute of Materials (London, England), Eds., *Engineering composite materials*, 2nd ed. in Book, no. 673. London: IOM, 2010.

[6] R. R. Nagavally, “COMPOSITE MATERIALS - HISTORY, TYPES, FABRICATION TECHNIQUES, ADVANTAGES, AND APPLICATIONS,” *Composite Materials*, 2016.

[7] K. K. Chawla, *Composite materials: science and engineering*, 3. ed., corr. At 2. printing. New York, NY: Springer, 2013.

[8] S. C. Hawkins, “Chapter 1 - Introduction to Fiber Materials,” in *Nanotube Superfiber Materials*, M. J. Schulz, V. N. Shanov, and Z. Yin, Eds., Boston: William Andrew Publishing, 2014, pp. 1–32. doi: 10.1016/B978-1-4557-7863-8.00001-3.

[9] M. W. Hyer and S. R. White, *Stress Analysis of Fiber-reinforced Composite Materials*. DEStech Publications, Inc, 2009.

[10] B. D. Agarwal, L. J. Broutman, and K. Chandrashekhara, *Analysis and Performance of Fiber Composites*. John Wiley & Sons, 2017.

[11] P. Bajpai, *Carbon Fibre from Lignin*. in SpringerBriefs in Materials. Singapore: Springer Singapore, 2017. doi: 10.1007/978-981-10-4229-4.

[12] E. G. Chatzi and J. L. Koenig, “Morphology and Structure of Kevlar Fibers: A Review,” *Polymer-Plastics Technology and Engineering*, vol. 26, no. 3–4, pp. 229–270, Sep. 1987, doi: 10.1080/03602558708071938.

[13] P. S, S. Km, N. K, and S. S, “Fiber Reinforced Composites - A Review,” *J Material Sci Eng*, vol. 06, no. 03, 2017, doi: 10.4172/2169-0022.1000341.

[14] R. F. Gibson, *Principles of composite material mechanics*, Fourth edition. Place of publication not identified: CRC Press, 2016.

[15] Z.-M. Dang, J.-K. Yuan, J.-W. Zha, T. Zhou, S.-T. Li, and G.-H. Hu, “Fundamentals, processes and

applications of high-permittivity polymer–matrix composites," *Progress in Materials Science*, vol. 57, no. 4, pp. 660–723, May 2012, doi: 10.1016/j.pmatsci.2011.08.001.

[16] D. B. Miracle, "Metal matrix composites – From science to technological significance," *Composites Science and Technology*, vol. 65, no. 15, pp. 2526–2540, Dec. 2005, doi: 10.1016/j.compscitech.2005.05.027.

[17] S. Suresh, *Fundamentals of Metal-Matrix Composites*. Elsevier, 2013.

[18] K. K. Chawla, "Ceramic Matrix Composites," in *Composite Materials: Science and Engineering*, K. K. Chawla, Ed., New York, NY: Springer, 2012, pp. 249–292. doi: 10.1007/978-0-387-74365-3_7.

[19] Z. Hua, Y. Liu, G. Yao, L. Wang, J. Ma, and L. Liang, "Preparation and Characterization of Nickel-Coated Carbon Fibers by Electroplating," *J. of Materi Eng and Perform*, vol. 21, no. 3, pp. 324–330, Mar. 2012, doi: 10.1007/s11665-011-9958-4.

[20] S. Ghosh, "Electroless copper deposition: A critical review," *Thin Solid Films*, vol. 669, pp. 641–658, Jan. 2019, doi: 10.1016/j.tsf.2018.11.016.

[21] A. Vardelle *et al.*, "The 2016 Thermal Spray Roadmap," *J Therm Spray Tech*, vol. 25, no. 8, pp. 1376–1440, Dec. 2016, doi: 10.1007/s11666-016-0473-x.

[22] D. H. Milanez, B. S. D. Oliveira, E. C. M. Noyons, L. I. L. Faria, and W. J. Botta, "Assessing Collaboration and Knowledge Flow on Coatings of Metallic Glasses Obtained From Thermal Spraying Processes Using Bibliometrics and Science Mapping," *Mat. Res.*, vol. 20, no. suppl 1, pp. 71–80, Nov. 2017, doi: 10.1590/1980-5373-mr-2017-0297.

[23] A. Vardelle, C. Moreau, N. J. Themelis, and C. Chazelas, "A Perspective on Plasma Spray Technology," *Plasma Chem Plasma Process*, vol. 35, no. 3, pp. 491–509, May 2015, doi: 10.1007/s11090-014-9600-y.

[24] H. Parmar, F. Tucci, P. Carlone, and T. S. Sudarshan, "Metallisation of polymers and polymer matrix composites by cold spray: state of the art and research perspectives," *International Materials Reviews*, vol. 67, no. 4, pp. 385–409, May 2022, doi: 10.1080/09506608.2021.1954805.

[25] G. O. Mallory and J. B. Hajdu, *Electroless Plating: Fundamentals and Applications*. William Andrew, 1990.

[26] A. Darvishzadeh and K. Nasouri, "Manufacturing, modeling, and optimization of nickel-coated carbon fabric for highly efficient EMI shielding," *Surface and Coatings Technology*, vol. 409, p. 126957, Mar. 2021, doi: 10.1016/j.surfcoat.2021.126957.

[27] W. Ohlhorst, L. Vaughn, and O. Ransone, "National Aeronautics and Space Administration Langley Research Center • Hampton, Virginia 23681-2199".

[28] "Copper and Nickel Coating of Carbon Fiber for Thermally and Electrically Conductive Fiber Reinforced Composites." Accessed: Nov. 20, 2024. [Online]. Available: https://www.mdpi.com/2073-

4360/11/5/823

[29]"Metals - Temperature Expansion Coefficients." Accessed: Nov. 15, 2024. [Online]. Available: https://www.engineeringtoolbox.com/thermal-expansion-metals-d_859.html

[30]A. Sparr, "Properties of Grade 5 Titanium (Ti6Al4V or Ti 6-4)," Parts Badger. Accessed: Jan. 26, 2024. [Online]. Available: https://parts-badger.com/properties-of-grade-5-titanium/

[31]D. C, L. K, J. Y, A. D, and Z. D, "Evaluation of thermal expansion coefficient of carbon fiber reinforced composites using electronic speckle interferometry," *Optics express*, vol. 26, no. 1, Aug. 2018, doi: 10.1364/OE.26.000531.

[32]W. D. Bascom, "The Surface Properties of Carbon Fibers and Their Adhesion to Organic Polymers".

[33]E. A. Clark, R. Yeske, and H. K. Birnbaum, "The effect of hydrogen on the surface energy of nickel," *Metall Trans A*, vol. 11, no. 11, pp. 1903–1908, Nov. 1980, doi: 10.1007/BF02655107.

[34]C. E. Bauer, R. Speiser, and J. P. Hirth, "Surface energy of copper as a function of oxygen activity," *Metall Trans A*, vol. 7, no. 1, pp. 75–79, Dec. 1976, doi: 10.1007/BF02644042.

[35]"04MAE 324 Structure & Properties of Engineering Materials 3 - RM24." Accessed: Nov. 15, 2024. [Online]. Available: https://www.princeton.edu/~maelabs/mae324/04/04mae_25.htm

[36]"AMERICAN ELEMENTS® | The Advanced Materials Manufacturer." Accessed: Nov. 22, 2024. [Online]. Available: https://www.americanelements.com

[37]PubChem, "Melting Point | Periodic Table of Elements." Accessed: Nov. 16, 2024. [Online]. Available: https://pubchem.ncbi.nlm.nih.gov/periodic-table/melting-point

[38]"(PDF) The Viscosity of Liquid-Metals and Alloys." Accessed: Nov. 16, 2024. [Online]. Available: https://www.researchgate.net/publication/223071408_The_Viscosity_of_Liquid-Metals_and_Alloys

[39]H. Parmar, F. Tucci, P. Carlone, and T. S. Sudarshan, "Metallisation of polymers and polymer matrix composites by cold spray: state of the art and research perspectives," *International Materials Reviews*, vol. 67, no. 4, pp. 385–409, May 2022, doi: 10.1080/09506608.2021.1954805.

[40]F. Faupel *et al.*, "Fundamental Aspects of Polymer Metallization," in *Metallization of Polymers 2*, E. Sacher, Ed., Boston, MA: Springer US, 2002, pp. 73–96. doi: 10.1007/978-1-4615-0563-1_8.

[41]R. Melentiev, A. Yudhanto, R. Tao, T. Vuchkov, and G. Lubineau, "Metallization of polymers and composites: State-of-the-art approaches," *Materials & Design*, vol. 221, p. 110958, Sep. 2022, doi: 10.1016/j.matdes.2022.110958.

[42]K. Seshan, *Handbook of Thin Film Deposition Techniques Principles, Methods, Equipment and Applications, Second Editon*. Boca Raton: CRC Press, 2014. doi: 10.1201/9781482269680.

[43]J. Audoit, L. Rivière, J. Dandurand, A. Lonjon, E. Dantras, and C. Lacabanne, "Thermal, mechanical and dielectric behaviour of poly(aryl ether ketone) with low melting temperature," *J Therm Anal Calorim*, vol. 135, no. 4, pp. 2147–2157, Feb. 2019, doi: 10.1007/s10973-018-7292-x.

[44]P. Fallah, S. Rajagopalan, A. McDonald, and S. Yue, “Development of hybrid metallic coatings on carbon fiber-reinforced polymers (CFRPs) by cold spray deposition of copper-assisted copper electroplating process,” *Surface and Coatings Technology*, vol. 400, p. 126231, Oct. 2020, doi: 10.1016/j.surfcoat.2020.126231.

[45]S. M. Tavana, M. Hojjati, A. C. Liberati, and C. Moreau, “Erosion resistance enhancement of polymeric composites with air plasma sprayed coatings,” *Surface and Coatings Technology*, vol. 455, p. 129211, Feb. 2023, doi: 10.1016/j.surfcoat.2022.129211.

[46]“ASM Handbook, Volume 5A: Thermal Spray Technology - ASM International.” Accessed: Jun. 20, 2024. [Online]. Available: https://www.asminternational.org/asm-handbook-volume-5a-thermal-spray-technology/results/-/journal_content/56/05348G/PUBLICATION/

[47]E. Petrovicova and L. S. Schadler, “Thermal spraying of polymers,” *International Materials Reviews*, vol. 47, no. 4, pp. 169–190, Aug. 2002, doi: 10.1179/095066002225006566.

[48]D. Tejero-Martin, M. Rezvani Rad, A. McDonald, and T. Hussain, “Beyond Traditional Coatings: A Review on Thermal-Sprayed Functional and Smart Coatings,” *J Therm Spray Tech*, vol. 28, no. 4, pp. 598–644, Apr. 2019, doi: 10.1007/s11666-019-00857-1.

[49]H. Koivuluoto, “A Review of Thermally Sprayed Polymer Coatings,” *J Therm Spray Tech*, vol. 31, no. 6, pp. 1750–1764, Aug. 2022, doi: 10.1007/s11666-022-01404-1.

[50]L. Pawlowski, *The science and engineering of thermal spray coatings*. Chichester, West Sussex: J. Wiley and sons, 2008.

[51]V. S. Bhattiprolu, K. W. Johnson, and G. A. Crawford, “Influence of Powder Heat Treatment on the Microstructure and Mechanical Properties of Cold Sprayed Ti-6Al-4V Coatings,” *J Therm Spray Tech*, vol. 30, no. 8, pp. 2050–2068, Dec. 2021, doi: 10.1007/s11666-021-01276-x.

[52]“What are the disadvantages of arc spraying?” Accessed: Jan. 04, 2025. [Online]. Available: https://www.twi-global.com/technical-knowledge/faqs/faq-what-are-the-disadvantages-of-arc-spraying.aspx

[53]P. L. Fauchais, J. V. R. Heberlein, and M. I. Boulos, “Overview of Thermal Spray,” in *Thermal Spray Fundamentals*, Boston, MA: Springer US, 2014, pp. 17–72. doi: 10.1007/978-0-387-68991-3_2.

[54]H. Che, P. Vo, and S. Yue, “Metallization of carbon fibre reinforced polymers by cold spray,” *Surface and Coatings Technology*, vol. 313, pp. 236–247, Mar. 2017, doi: 10.1016/j.surfcoat.2017.01.083.

[55]A. C. Liberati, H. Che, P. Fallah, P. Vo, and S. Yue, “Pull-off Testing and Electrical Conductivity of Sn-Based Metal Powder Mixtures Cold Sprayed on Carbon Fiber-Reinforced Polymers,” *J Therm Spray Tech*, vol. 31, no. 6, pp. 1792–1812, Aug. 2022, doi: 10.1007/s11666-022-01405-0.

[56]S. Green *et al.*, “VICTREX AE™ 250 UDT – UNIQUE PAEK PREPREG ALLOWS FAST & EFFICIENT COMPOSITE PARTS MANUFACTURE”.

[57]A. M. Tarditi, M. L. Bosko, and L. M. Cornaglia, “3.1 Electroless Plating of Pd Binary and Ternary Alloys and Surface Characteristics for Application in Hydrogen Separation,” in *Comprehensive Materials Finishing*, M. Hashmi, Ed., Oxford: Elsevier, 2017, pp. 1–24. doi: 10.1016/B978-0-12-803581-8.09166-9.

[58]S. Nihtianov and A. Luque, Eds., *Smart sensors and MEMS: intelligent devices and microsystems for industrial applications*. in Woodhead Publishing series in electronic and optical materials, no. 51. Oxford: Woodhead Publishing, 2014.

[59]M. A. Azmah Hanim, “3.15 Electroless Plating as Surface Finishing in Electronic Packaging,” in *Comprehensive Materials Finishing*, M. Hashmi, Ed., Oxford: Elsevier, 2017, pp. 220–229. doi: 10.1016/B978-0-12-803581-8.09177-3.

[60]C. Lyphout, “Internal Diameter HVAF Spraying for Wear and Corrosion Applications,” Jan. 2014, Accessed: Jan. 04, 2025. [Online]. Available: https://www.academia.edu/62933204/Internal_Diameter_HVAF_Spraying_for_Wear_and_Corrosion_Applications

[61]“Ti-6AI-4V Gr. 5,” Advanced Powders. Accessed: Jan. 26, 2024. [Online]. Available: https://www.ge.com/powders/titanium/ti-6al-4v-5

[62]“CenterLine Supersonic Spray Technology - SST™ Powders.” Accessed: Dec. 22, 2024. [Online]. Available: https://www.supersonicspray.com/products/sst-powders

[63]V. Genova, L. Paglia, F. Marra, C. Bartuli, and G. Pulci, “Pure thick nickel coating obtained by electroless plating: Surface characterization and wetting properties,” *Surface and Coatings Technology*, vol. 357, pp. 595–603, Jan. 2019, doi: 10.1016/j.surfcoat.2018.10.049.

[64]I. Ohno, “Electrochemistry of electroless plating,” *Materials Science and Engineering: A*, vol. 146, no. 1, pp. 33–49, Oct. 1991, doi: 10.1016/0921-5093(91)90266-P.

[65]C. G. Jothi Prakash and R. Prasanth, “Approaches to design a surface with tunable wettability: a review on surface properties,” *J Mater Sci*, vol. 56, no. 1, pp. 108–135, Jan. 2021, doi: 10.1007/s10853-020-05116-1.

[66]D. W. Baudrand, “Do’s and don’ts of electroless nickel plating: Solutions using sodium hypophosphite,” vol. 94, pp. 24–25, Aug. 2007.

[67]Xiao Qin, G. Lin, J. Wang, K. Zheng, and X. Feng, “Effect of pH Value on Electroless Deposition of Copper Graphite Powders,” *Prot Met Phys Chem Surf*, vol. 57, no. 1, pp. 132–138, Jan. 2021, doi: 10.1134/S2070205120060192.

[68]N. V. Mandich, G. A. Krulik, and R. Singh, “Electroless silver plating composition,” US5322553A, Jun. 21, 1994 Accessed: Dec. 22, 2024. [Online]. Available: https://patents.google.com/patent/US5322553A/en

[69]J. Mostaghimi and S. Chandra, “Droplet Impact and Solidification in Plasma Spraying,” in *Handbook of Thermal Science and Engineering*, Cham: Springer International Publishing, 2018, pp. 2967–3008. doi: 10.1007/978-3-319-26695-4_78.

[70]H. Zhang, X. Y. Wang, L. L. Zheng, and X. Y. Jiang, “Studies of splat morphology and rapid solidification during thermal spraying,” *International Journal of Heat and Mass Transfer*, vol. 44, no. 24, pp. 4579–4592, Dec. 2001, doi: 10.1016/S0017-9310(01)00109-0.

[71]O. Kovářík *et al.*, “The influence of substrate temperature on properties of APS and VPS W coatings,” *Surface and Coatings Technology*, vol. 268, pp. 7–14, Apr. 2015, doi: 10.1016/j.surfcoat.2014.07.041.

[72]H. B. Guo, R. Vaßen, and D. Stöver, “Atmospheric plasma sprayed thick thermal barrier coatings with high segmentation crack density,” *Surface and Coatings Technology*, vol. 186, no. 3, pp. 353–363, Sep. 2004, doi: 10.1016/j.surfcoat.2004.01.002.

[73]“Melting Points of Common Materials | Toolbox | AMERICAN ELEMENTS ®,” American Elements: The Materials Science Company. Accessed: Dec. 22, 2024. [Online]. Available: https://www.americanelements.com/meltingpoint.html

[74]L. Yang, Y. Zhang, and J. K. Chen, “Molecular dynamics simulation of deposition of nickel nanocluster on copper surface,” *J Nanopart Res*, vol. 13, no. 10, pp. 4479–4489, Oct. 2011, doi: 10.1007/s11051-011-0400-5.

[75]B. Medasani, Y. H. Park, and I. Vasiliev, “Theoretical study of the surface energy, stress, and lattice contraction of silver nanoparticles,” *Phys. Rev. B*, vol. 75, no. 23, p. 235436, Jun. 2007, doi: 10.1103/PhysRevB.75.235436.

[76]Y. X. Ni, B. Feng, J. Wang, X. Lu, S. Qu, and J. Weng, “Decyl bis phosphonate–protein surface modification of Ti–6Al–4V via a layer-by-layer technique,” *J Mater Sci*, vol. 44, no. 15, pp. 4031–4039, Aug. 2009, doi: 10.1007/s10853-009-3562-0.

[77]“(PDF) The Initial Oxidation of HfNiSn Half-Heusler Alloy by Oxygen and Water Vapor,” *ResearchGate*, Dec. 2024, doi: 10.3390/ma14143942.

[78]S. Bard, F. Schönl, M. Demleitner, and V. Altstädt, “Copper and Nickel Coating of Carbon Fiber for Thermally and Electrically Conductive Fiber Reinforced Composites,” *Polymers (Basel)*, vol. 11, no. 5, p. 823, May 2019, doi: 10.3390/polym11050823.

[79]“Metals - Temperature Expansion Coefficients.” Accessed: Feb. 06, 2024. [Online]. Available: https://www.engineeringtoolbox.com/thermal-expansion-metals-d_859.html

[80]“Coefficient of Thermal Expansion.” Accessed: Jan. 04, 2025. [Online]. Available: http://www.repairengineering.com/coefficient-of-thermal-expansion.html

[81]“Metals - Latent Heat of Melting.” Accessed: Dec. 26, 2024. [Online]. Available: https://www.engineeringtoolbox.com/fusion-heat-metals-d_1266.html

[82]J. L. McClure and A. Cezairliyan, “Measurement of the heat of fusion of titanium and a titanium alloy (90Ti-6Al-4V) by a microsecond-resolution transient technique,” *Int J Thermophys*, vol. 13, no. 1, pp. 75–81, Jan. 1992, doi: 10.1007/BF00503357.

[83]E. Edge and E. E. LLC, “Specific Heat Capacity of Metals Table Chart.” Accessed: Dec. 26, 2024. [Online]. Available: https://www.engineersedge.com/materials/specific_heat_capacity_of_metals_13259.htm

[84]“ASM Material Data Sheet.” Accessed: Dec. 26, 2024. [Online]. Available: https://asm.matweb.com/search/specificmaterial.asp?bassnum=mtp642

[85]M. Molteni, M. Bona, A. Chierichetti, G. Trecordi, and E. Gariboldi, “Microstructural Suitability and Stability of AlSi10Mg–Sn Plasma Coatings for Thermal Energy Storage Purposes,” *Metals*, vol. 14, no. 12, Art. no. 12, Dec. 2024, doi: 10.3390/met14121414.

[86]D. Bonn, J. Eggers, J. Indekeu, J. Meunier, and E. Rolley, “Wetting and spreading,” *Rev. Mod. Phys.*, vol. 81, no. 2, pp. 739–805, May 2009, doi: 10.1103/RevModPhys.81.739.

[87]“Wettability - an overview | ScienceDirect Topics.” Accessed: Jan. 15, 2025. [Online]. Available: https://www.sciencedirect.com/topics/materials-science/wettability

[88]S. Chandra and P. Fauchais, “Formation of Solid Splats During Thermal Spray Deposition,” *J Therm Spray Tech*, vol. 18, no. 2, pp. 148–180, Jun. 2009, doi: 10.1007/s11666-009-9294-5.

[89]“Introduction to Surface Energy | 3M Science of Adhesion Educational Series.” Accessed: Jan. 15, 2025. [Online]. Available: https://www.3m.com/3M/en_US/bonding-and-assembly-us/resources/science-of-adhesion/introduction-surface-energy/

[90]“ID gun to spray wear resistant carbide coatings onto Internal diameters.” Accessed: Jan. 04, 2025. [Online]. Available: https://kermetico.com/ak/internal-diameter-metal-carbide-spray-id-gun-wear-protection-coating

[91]M. A. Shakir, B. Azahari, Y. Yusup, M. F. Yhaya, A. Salehabadi, and M. I. Ahmad, “Preparation and Characterization of Mycelium as a Bio-Matrix in Fabrication of Bio-Composite,” *Journal of Advanced Research in Fluid Mechanics and Thermal Sciences*, vol. 65, no. 2, Art. no. 2, 2020.

[92]J. Zhu, “Development of novel flax bio-matrix composites for non-structural and structural vehicle applications,” 2015, Accessed: Nov. 28, 2024. [Online]. Available: http://dspace.lib.cranfield.ac.uk/handle/1826/9223

[93]A. R. Govande, A. Chandak, B. R. Sunil, and R. Dumpala, “Carbide-based thermal spray coatings: A review on performance characteristics and post-treatment,” *International Journal of Refractory Metals and Hard Materials*, vol. 103, p. 105772, Feb. 2022, doi: 10.1016/j.ijrmhm.2021.105772.

[94]I. Zvonkina and M. Soucek, “Inorganic–organic hybrid coatings: common and new approaches,” *Current Opinion in Chemical Engineering*, vol. 11, pp. 123–127, Feb. 2016, doi:

10.1016/j.coche.2016.01.008.

[95]M. Nurhaniza, M. K. A. Ariffin, A. Ali, F. Mustapha, and A. W. Noraini, “Finite element analysis of composites materials for aerospace applications,” *IOP Conf. Ser.: Mater. Sci. Eng.*, vol. 11, no. 1, p. 012010, May 2010, doi: 10.1088/1757-899X/11/1/012010.

[96]P. Mahendru, M. Tembely, and A. Dolatabadi, “Artificial Intelligence Models for Analyzing Thermally Sprayed Functional Coatings,” *J Therm Spray Tech*, vol. 32, no. 2, pp. 388–400, Mar. 2023, doi: 10.1007/s11666-023-01554-w.